Energy & Environmental Science

PERSPECTIVE

View Article Online
View Journal | View Issue

Cite this: *Energy Environ. Sci.*, 2018, **11**, 2784

An assessment of strategies for the development of solid-state adsorbents for vehicular hydrogen storage

Mark D. Allendorf, *[a] Zeric Hulvey,*[bc] Thomas Gennett,[de] Alauddin Ahmed,[f] Tom Autrey,[g] Jeffrey Camp,[h] Eun Seon Cho,[p] Hiroyasu Furukawa,[ij] Maciej Haranczyk,[h] Martin Head-Gordon,[ik] Sohee Jeong,[jo] Abhi Karkamkar,[g] Di-Jia Liu,[l] Jeffrey R. Long,[ijm] Katie R. Meihaus,[i] Iffat H. Nayyar,[g] Roman Nazarov,[n] Donald J. Siegel,[f] Vitalie Stavila,[a] Jeffrey J. Urban,[o] Srimukh Prasad Veccham[i] and Brandon C. Wood[n]

Nanoporous adsorbents are a diverse category of solid-state materials that hold considerable promise for vehicular hydrogen storage. Although impressive storage capacities have been demonstrated for several materials, particularly at cryogenic temperatures, materials meeting all of the targets established by the U.S. Department of Energy have yet to be identified. In this Perspective, we provide an overview of the major known and proposed strategies for hydrogen adsorbents, with the aim of guiding ongoing research as well as future new storage concepts. The discussion of each strategy includes current relevant literature, strengths and weaknesses, and outstanding challenges that preclude implementation. We consider in particular metal–organic frameworks (MOFs), including surface area/volume tailoring, open metal sites, and the binding of multiple H_2 molecules to a single metal site. Two related classes of porous framework materials, covalent organic frameworks (COFs) and porous aromatic frameworks (PAFs), are also discussed, as are graphene and graphene oxide and doped porous carbons. We additionally introduce criteria for evaluating the merits of a particular materials design strategy. Computation has become an important tool in the discovery of new storage materials, and a brief introduction to the benefits and limitations of computational predictions of H_2 physisorption is therefore presented. Finally, considerations for the synthesis and characterization of hydrogen storage adsorbents are discussed.

Received 12th April 2018,
Accepted 17th July 2018

DOI: 10.1039/c8ee01085d

rsc.li/ees

Introduction

Storage of hydrogen with sufficient gravimetric and volumetric capacity for vehicular use remains a significant obstacle to the widespread adoption of hydrogen fuel cell electric vehicles (FCEVs). Several FCEV models are now commercially available in limited locations around the world, and in these vehicles hydrogen is stored as a gas at room temperature with a fill

[a] *Energy & Transport Technology Center, Sandia National Laboratories, Livermore, CA 94551, USA. E-mail: mdallen@sandia.gov*
[b] *Fuel Cell Technologies Office, U.S. Department of Energy Office of Energy Efficiency and Renewable Energy, Washington, DC 20585, USA. E-mail: Zeric.Hulvey@hq.doe.gov*
[c] *Oak Ridge Institute for Science and Education, Washington, DC 20585, USA*
[d] *Department of Chemistry, Colorado School of Mines, Golden, CO 80401, USA*
[e] *National Renewable Energy Laboratory, Golden, CO 80401, USA*
[f] *Mechanical Engineering Department, University of Michigan, Ann Arbor, Michigan 48109, USA*
[g] *Pacific Northwest National Laboratory, Richland, WA 99354, USA*
[h] *Computational Research Division, Lawrence Berkeley National Laboratory, Berkeley, CA 94720, USA*
[i] *Department of Chemistry, University of California, Berkeley, CA 94720, USA*
[j] *Materials Sciences Division, Lawrence Berkeley National Laboratory, Berkeley, CA 94720, USA*
[k] *Chemical Sciences Division, Lawrence Berkeley National Laboratory, Berkeley, CA 94720, USA*
[l] *Chemical Sciences and Engineering Division, Argonne National Laboratory, Lemont, IL 60439, USA*
[m] *Department of Chemical and Biomolecular Engineering, University of California, Berkeley, CA 94720, USA*
[n] *Lawrence Livermore National Laboratory, Livermore, CA 94550, USA*
[o] *Molecular Foundry, Lawrence Berkeley National Laboratory, Berkeley, CA 94720, USA*
[p] *Department of Chemical and Biomolecular Engineering, Korea Advanced Institute of Science and Technology (KAIST), Korea*

Broader context

The widespread use of hydrogen as a clean, sustainable energy carrier has the potential to provide several significant benefits, including a reduction in oil dependency and emissions, improved energy security and grid resiliency, and substantial economic opportunities across many sectors. Hydrogen-fueled vehicles are already appearing internationally, and one of the critical enabling technologies for increasing their availability is on-board hydrogen storage. Stakeholders in developing a hydrogen infrastructure (*e.g.*, state governments, automotive manufacturers, station providers, and industrial gas suppliers) are currently focused on high-pressure storage of H_2 at 350 and 700 bar, in part because no viable hydrogen storage material has emerged. Novel adsorbents are an important category of storage materials that have attracted considerable interest because of their potential to meet all DOE targets and deliver hydrogen at lower pressures and higher on-board densities. Nevertheless, the most promising materials synthesized to date require cryogenic temperatures to maximize their capacity, and storage under such conditions is undesirable because it adds complexity and cost to the fuel delivery system. Consequently, a successful solid-state materials solution would significantly reduce costs and ensure the economic viability of a U.S. hydrogen infrastructure.

pressure of 700 bar. The carbon fiber-reinforced H_2 tanks used in these vehicles are expensive, and the compression and pre-cooling requirements that are necessary to deliver 700 bar of H_2 at the station add significant penalties with regard to cost, reliability, and energy consumption.[1] The U.S. Department of Energy (DOE), in conjunction with U.S. DRIVE (Driving Research and Innovation for Vehicle Efficiency and Energy), a public–private partnership between DOE and automotive, energy, and utility companies, has developed a comprehensive set of hydrogen storage system targets for light-duty vehicles to enable widespread commercialization of FCEVs.[2] A few of the most relevant targets are listed in Table 1 along with the current performance of 700 bar systems. These values pertain to the entire storage system, which includes the mass and volume of hydrogen in addition to the tank and associated balance-of-plant (BOP) components. Notably, it is physically impossible to meet the 2025 and ultimate volumetric capacity target with pressurized gas, as the density of H_2 gas at 700 bar and room temperature is just 40 g L^{-1} without accounting for the BOP.

The search for solid-state H_2 storage materials that can supplant compressed gas systems has been ongoing for at least two decades. The development of a viable storage material

Mark D. Allendorf

Mark Allendorf is Director of the Hydrogen Advanced Materials Research Consortium (HyMARC) and a senior scientist at Sandia National Laboratories. He received an AB degree in chemistry from Washington University in St. Louis and a PhD degree in chemistry from Stanford University. His research focuses on the fundamental science and applications of metal–organic frameworks and related materials. He has been published in more than 160 publications, including more than 120 journal articles. He is President Emeritus and Fellow of The Electrochemical Society and his awards include a 2014 R&D 100 Award for a novel approach to radiation detection.

Zeric Hulvey

Zeric Hulvey is an ORISE research fellow in the Fuel Cell Technologies Office of the U.S. Department of Energy's Office of Energy Efficiency and Renewable Energy. He received his PhD in Inorganic Chemistry in 2010 from the University of California, Santa Barbara in the group of Prof. A. K. Cheetham FRS, and carried out postdoctoral work with Craig M. Brown at the NIST Center for Neutron Research. His research background involves the synthesis and structural characterization of metal–organic frameworks for gas adsorption applications. In his current role, he provides technical project analysis for FCTO's portfolio of materials-based hydrogen storage projects.

Thomas Gennett

Thomas Gennett holds a joint appointment as a Professor of Chemistry/Department Head at the Colorado School of Mines and serves as a Principal Scientist at NREL. He is currently the PI and co-Director of the Hydrogen Materials Advanced Research Consortium (HyMARC). His research interests include hydrogen storage characterization and optimization, fundamental charge transfer processes in stable free-radical organic polymer material systems, non-pgm catalysts, and hybrid hard–soft materials for energy storage. Prof. Gennett holds a BA in chemistry from the State University of New York at Potsdam and a PhD in Analytical Chemistry from the University of Vermont. He was a professor of chemistry and materials Science at Rochester Institute of Technology for 18 years and holds the title of emeritus.

Table 1 U.S. Department of Energy onboard H_2 storage targets compared to the performance of 700 bar compressed storage technology. Costs are projected at 500 000 units per year

Target[2] or status	System gravimetric capacity (wt% H_2)	System volumetric capacity (g per L H_2)	Cost ($ per kW h)
2020 targets	4.5	30	10
2025 targets	5.5	40	9
Ultimate targets	6.5	50	8
700 bar compressed[3]	4.2	24	15

would enable increased system-level capacities, thereby resulting in a reduction of the mass, volume, and cost requirements of the storage system. Furthermore, materials-based storage would enable lower operating pressures and potentially reduce other requirements such as pre-cooling at the fueling station, providing additional cost and energy savings to the driver. Among the various types of storage materials, porous adsorbents have the potential to offer rapid filling times and delivery response, long cycle life, and easily-controlled delivery pressures. However, several challenges remain in the development and implementation of such materials: both volumetric and gravimetric capacities for the best performing adsorbents are still well below the DOE targets (Table 1) and usable, system-level capacities can be significantly less than total uptake for a given material. Furthermore, it is difficult to extrapolate system-level performance from the typical laboratory measurements carried out to investigate adsorption properties for a given material. Several material design strategies have been proposed to address these challenges, and in 2010 the DOE-funded Hydrogen Sorption Center of Excellence (HSCoE) produced a report with recommendations for continuing material development efforts (see discussion below).[4] Since then, the science of hydrogen storage has advanced considerably and some of these earlier recommendations are no longer valid while others have been amplified by subsequent discoveries. Moreover, new strategies have been proposed in recent years, some of which have received only cursory attention.

The objective of this Perspective is to evaluate the various current known and proposed strategies for improving the performance of hydrogen adsorbents, with an eye toward guiding current and ongoing research, as well as proposals to develop new storage concepts. This work also includes essential updates to the conclusions of the 2010 HSCoE report. In our analysis, the primary focus is on optimizing properties that currently represent major impediments to successful materials implementation, namely low isosteric heats of adsorption (Q_{st}) and sub-par usable volumetric and gravimetric capacities. Clearly, there are other material properties that could significantly impact performance, such as material stability, durability, cyclability, adsorption kinetics, packing density, and system engineering effects; however, to include all of these criteria here is impractical. Consequently, we provide a short discussion of the most pertinent practical metrics for evaluating material utility and the various caveats associated with their optimization.

Theory and modeling are now valuable tools for guiding the design of new materials and for characterizing their performance, and hydrogen adsorbents are no exception. Advances in theory and computing power have greatly improved upon earlier models and in some cases have revised the conclusions of previous results. We deemed it important to also provide an abbreviated overview of theoretical methods and predictions and how they compare with current experiment-based understanding. Recommended methods and levels of theory considered to be the best for modeling specific aspects of adsorbent behavior are discussed. In particular, we address the demanding problem of accurately modeling the interaction energy of H_2 with strongly binding sites in metal–organic frameworks (MOFs) and the accuracy of force fields used in atomistic modeling to predict H_2 adsorption isotherms.

Finally, we provide guidance concerning the feasibility of synthesizing novel adsorbents, and the potential drawbacks associated with characterization tools used to evaluate them. As in the sections on theory and materials properties, this synthesis section is a concise summary rather than a comprehensive review. Our intention is ultimately to raise awareness of potential key issues so that they can be avoided in future research efforts and when reporting results.

Materials evaluation criteria

Usable gravimetric and volumetric capacities

As a starting point, it is useful to briefly address how the target quantities in Table 1 relate to material performance. As stated earlier, these targets are based on the entire storage system, and do not correspond to material-specific properties. Moreover, there can be a significant difference between usable capacity, *i.e.*, H_2 that is actually accessible to power the vehicle, and total or excess capacity, which is more typically measured and reported for adsorbents.[5] The difference between these two capacities is illustrated in Fig. 1, in which total volumetric H_2 uptake *versus* pressure data is plotted for a hypothetical storage material. The dashed lines correspond to pressures of 5 and 100 bar, which are the pressure bounds typically used for estimating usable capacity in adsorbents. The lower value of 5 bar is a DOE target for the minimum pressure required to deliver H_2 to the fuel cell system (the "discharged state"), and the pressure at which the system is fully charged in this case is 100 bar (the "charged state", or refueling pressure). A refueling pressure of 100 bar is often used to determine usable capacity because it represents the pressure below which an all-metal Type I pressure vessel can be used, imparting significant cost savings over other types of carbon-fiber overwrapped vessels necessary for higher pressure operation.[6,7] At the lower pressure end of the isotherm, it is evident that some of the stored H_2 is not available for use because the tank pressure

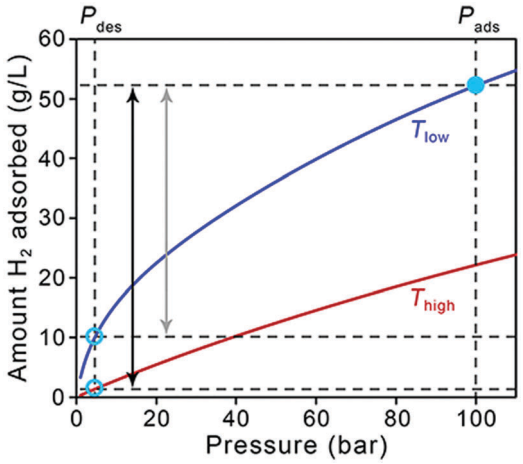

Fig. 1 Illustration of usable volumetric capacity for a hypothetical storage material. Total volumetric adsorption isotherms are shown as red and blue curves, corresponding to high and low temperatures respectively. The "charged" state is represented by a filled pale blue circle and the "discharged" state is represented by open pale blue circles. Black and grey double-sided arrows represent volumetric usable capacities achieved for temperature–pressure swing or only pressure swing adsorption processes, respectively, with P_{ads} = 100 bar and P_{des} = 5 bar.

is below the lower operating limit of 5 bar. The magnitude of this unused H_2 can be substantial for materials with high adsorption energies, *i.e.*, those for which the slope of the isotherm (the Henry's constant in the linear region) is steep at pressures below 5 bar.

Storage temperature is another complicating factor, and Fig. 1 also illustrates how the usable capacity of H_2 in a given material can change with operating temperature (red and blue curves). As the DOE targets only address hydrogen delivery temperature (−40 to 85 °C, to meet fuel cell system operation specifications) and not the storage system operating temperature, a range of possible system designs can be considered. Materials-based systems designed to operate at lower temperatures may require more complex and costly BOP components (*e.g.*, thermal insulation, heat exchangers) and will therefore likely impart more penalties on the system-level capacity compared to systems designed to operate at ambient temperatures.[8] Adsorbent systems could also incorporate a temperature swing step, for example from 77 to 160 K, which increases usable capacities by increasing the quantity of H_2 desorbed upon cycling. Systems operating at lower temperatures will also likely require materials with significantly higher capacities compared to ambient temperature systems to compensate for insulation and additional system complexity; unfortunately, there is no simple factor that can be applied to quantify this requirement. Tank design aspects constitute more of an engineering challenge than a materials challenge, and we will not address them in detail here. While it is important to keep operating temperature in mind when comparing the behavior of different adsorbents, it is not necessary to discount a specific class of materials specifically because of operating temperature—the focus herein is on material strategies to increase capacities for any adsorbent.

Historically, much of the early focus on materials development was toward maximizing adsorbent surface area to achieve the necessary gravimetric capacities, and the discovery of ultrahigh surface area materials such as the MOF NU-100 (reported Brunauer–Emmett–Teller [BET] surface area of 6143 m^2 g^{-1}) generated excitement that the DOE targets could soon be met.[9] This optimism was supported by empirical observations that maximum excess gravimetric capacity increased approximately linearly with increasing surface area, at the rate of ~1 wt% per 500 m^2 g^{-1} for adsorption at 77 K and moderate pressures of ~35 bar, commonly referred to as Chahine's rule.[10,11] There are some exceptions to this rule, for example in selected carbons an increase in pore size can result in a net decrease in gravimetric H_2 uptake, even though the surface area increases.[12] Adsorbents that demonstrate very strong binding of H_2 can also exhibit gravimetric capacities that exceed those predicted by this relationship.

As more high surface area materials were synthesized, it became apparent that exceptional gravimetric capacity often comes at the expense of volumetric capacity. This relationship was reported by Siegel and coworkers, who analyzed the trend between total volumetric and gravimetric capacity calculated for ~4000 porous materials extracted from the Cambridge Structural Database (Fig. 2). Notably, the authors found that total volumetric capacity is at a maximum for materials with surface areas ranging from 3100–4800 m^2 g^{-1}.[13] It is unclear whether the trade-off between gravimetric and volumetric capacities represents a peculiarity specific to materials that have been synthesized to date, or instead reflects a universal feature of H_2 uptake in adsorbents. Subsequent reports have highlighted the effect of hydrogen storage densities on driving range; these analyses argue that FCEV driving range is more strongly tied to volumetric capacity than gravimetric capacity.[6,14,15] Adsorbents with exceptional gravimetric capacities may therefore not be very attractive from a systems-level standpoint, and it is essential that both gravimetric and volumetric capacity be considered simultaneously when analyzing the viability of a specific adsorbent.

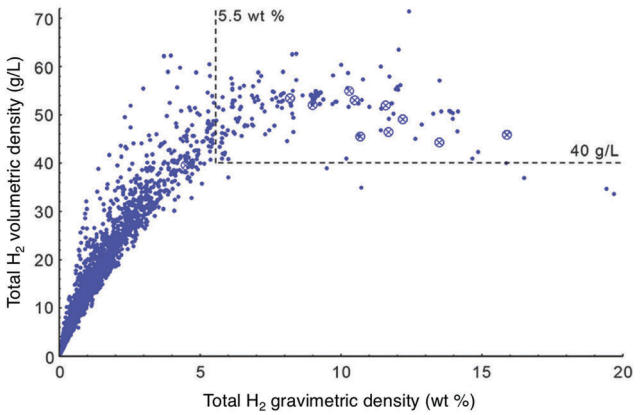

Fig. 2 Theoretical total volumetric *vs.* gravimetric capacities for various materials at 77 K and 35 bar, compared with the DOE 2025 system targets (5.5 wt% and 40 g L^{-1}, as outlined by dashed lines). Adapted with permission from J. Goldsmith, A. G. Wong-Foy, M. J. Cafarella and D. J. Siegel, *Chem. Mater.*, 2013, **25**, 3373. Copyright 2008 American Chemical Society.

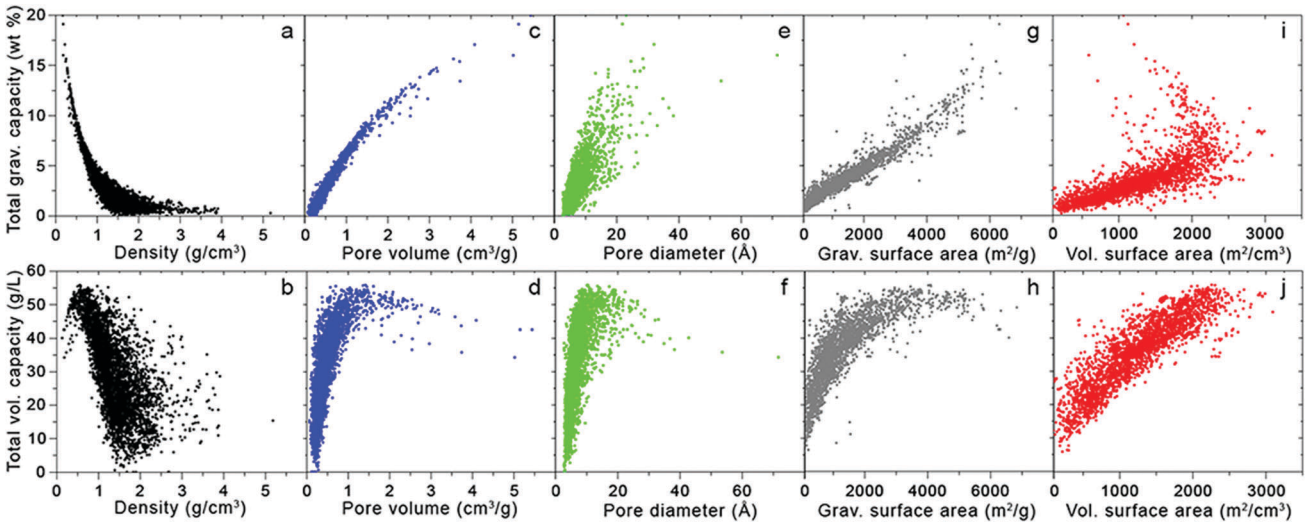

Fig. 3 Total gravimetric (top) and volumetric (bottom) capacities as a function of various crystallographic properties for 5309 MOFs extracted from the UM and CoRE databases.[13,16] Capacities were calculated at 77 K and 100 bar using Grand Canonical Monte Carlo (GCMC) simulations with the pseudo-Feynman–Hibbs interatomic potential.[17–19]

Fig. 3 takes these analyses a step further by illustrating the dependence of H_2 uptake on adsorbent structural features; here, the simulated total volumetric and gravimetric capacities of a database of MOFs[13,14,16] are plotted with respect to five crystallographic properties: density, pore volume, pore diameter (defined as the largest diameter of any internal cavity), gravimetric surface area, and volumetric surface area. The total capacities approximate the usable capacities that could be achieved using a combined temperature–pressure swing process, from $T = 77$ K and $P = 100$ bar to $T = 160$ K and $P = 5$ bar. Thus, as mentioned above, these total capacities correspond to an upper limit for the amount of H_2 that could be delivered by the given material storage system. The ranges of these crystallographic properties that optimize gravimetric and volumetric performance are summarized in Table 2.

Turning first to the dependence of total capacity on MOF density, Fig. 3a shows that gravimetric capacity monotonically decreases with increasing density. In contrast, total volumetric capacity (Fig. 3b) first increases as density increases from zero to $\sim$0.5 g cm^{-3}, but then drops off for higher densities. These data suggest that maximizing gravimetric and volumetric performance simultaneously can be achieved with densities between 0.4 and 0.5 g cm^{-3}.

With both increasing pore volume and diameter, the gravimetric capacity increases monotonically (Fig. 3c and e, respectively), although the trend is more pronounced in the case of pore volume (Fig. 3c), as might be expected given Chahine's rule (albeit at a higher pressure of 100 bar). The total volumetric capacity displays a non-monotonic dependence on both pore volume and diameter (Fig. 3d and f, respectively), initially increasing with increasing volume and diameter to reach a maximum value for volumes between 1 and 2 cm^3 g^{-1} and diameters between 10 and 20 Å, before decreasing for larger values.

The influence of gravimetric and volumetric surface area on H_2 capacity is illustrated in Fig. 3g–j. As expected from Chahine's rule, gravimetric capacity correlates roughly linearly with gravimetric surface area (Fig. 3g). In contrast, the relationship between total volumetric capacity and gravimetric surface area (Fig. 3h) is reminiscent of that observed in Fig. 2: MOFs with very high surface areas (coinciding with large gravimetric capacities) tend to exhibit poor volumetric performance.[13] From this data, it is clear that MOFs with gravimetric surface areas ranging from 4500 to 5500 m^2 g^{-1} present a reasonable compromise in balancing gravimetric and volumetric performance. Unsurprisingly, volumetric capacity increases with volumetric surface area in a linear fashion (Fig. 3j), with the highest capacities exhibited by MOFs with surface areas $>$2000 m^2 cm^{-3}. The relationship between gravimetric capacity and volumetric surface area is more complex: although the capacity of most MOFs increases linearly with increasing surface area, the highest capacities are exhibited by several materials with volumetric surface areas in the range of 1000–2000 m^2 g^{-1}. Thus, volumetric surface areas between 1500 and 2250 m^2 g^{-1} serve to maximize both gravimetric and volumetric performance.

Additional studies have examined this interplay between gravimetric and volumetric capacities and suggested ranges similar to those given in Table 2 for structural properties that optimize adsorptive H_2 storage at cryogenic conditions.[20–23] For example, Thornton and coworkers trained a neural network to predict hydrogen uptake across a diverse collection of adsorbents, including MOFs, covalent organic frameworks (COFs), zeolites, zeolitic imidizolate frameworks (ZIFs), and porous polymer networks.[20,24] Their model identified several MOFs as amongst the highest capacity materials, with predicted optimal ranges for pore diameter and surface area that closely match those from the MOF-only dataset represented by Fig. 3 and Table 2. This result suggests that these ranges may serve as a reasonable approximation for target structural features in other non-MOF classes of adsorbents, at least under cryogenic conditions.

Can additional optimization of the intrinsic framework structural features increase capacity even more? Metal–organic

Table 2 Ranges of various crystallographic properties that optimize gravimetric and volumetric H_2 uptake in MOFs at 77 K and 100 bar based on the study by Siegel and team (ref. 14)

Crystallographic metric	Range
Density (g cm^{-3})	0.4–0.5
Pore volume (cm^3 g^{-1})	1–2
Pore diameter (Å)	10–20
Gravimetric surface area (m^2 g^{-1})	4500–5500
Volumetric surface area (m^2 cm^{-3})	1500–2250

frameworks already excel on a gravimetric basis, as seen in Fig. 3, with some compounds predicted to exhibit capacities exceeding 15 wt%. On the other hand, under the cryogenic conditions utilized in this study, no known MOFs exhibit total volumetric capacities exceeding 60 g L^{-1}. Given that some MOFs exhibit adsorbed H_2 densities comparable to that of liquid or solid H_2 (70–76 g L^{-1}), a lofty goal would be to achieve these densities on a total capacity basis, *i.e.*, factoring in both adsorbed and gas-phase H_2. Thus, developing new MOFs that improve volumetric performance, without sacrificing high gravimetric density, presents one path forward.

The importance of binding strength

While structural features clearly influence the packing of H_2 within an adsorbent, of equal importance are the specific binding locations within the pores and the relative binding strength at these sites. The interaction of H_2 with the adsorbent surface is commonly quantified by the enthalpy of adsorption (ΔH) or the isosteric heat of adsorption (Q_{st}), and these values should typically follow the relationship $\Delta H = -Q_{st}$. We note that no strict convention is used when reporting the isosteric heat of adsorption, and it can be given either as $-Q_{st}$ (values >0) or simply Q_{st} (values <0), and in subsequent discussion we report the values as originally reported in the respective publications. These parameters differ slightly in the manner in which they are derived from experimental data and are used somewhat interchangeably by those in the field, although the differential enthalpy of adsorption at zero coverage is most commonly reported, where the gas concentration varies linearly with pressure.[11] Since the adsorption enthalpy typically varies as a function of H_2 uptake, for practical applications the average ΔH is more important than the low coverage Henry's law enthalpy value, and for most adsorbents the enthalpy of adsorption is expected to decay monotonically with increasing H_2 coverage.[25]

At temperatures and pressures above its boiling point, the first monolayer of H_2 adsorbed at a solid surface typically exhibits adsorption enthalpies in the range of ~1–10 kJ mol^{-1}.[26] While adsorption enthalpies are reported on a rather limited basis due to measurement challenges, available literature data indicate that enthalpies larger than 10 kJ mol^{-1} are relatively rare and are mainly found in doped carbons,[27] functionalized zeolites,[28] and MOFs[29] with structural features that impart strong metal–hydrogen interactions (Fig. 4). Examples of some of these materials will be described in detail later in this Perspective. The available literature adsorption enthalpies can be investigated as a function of gravimetric capacity as shown

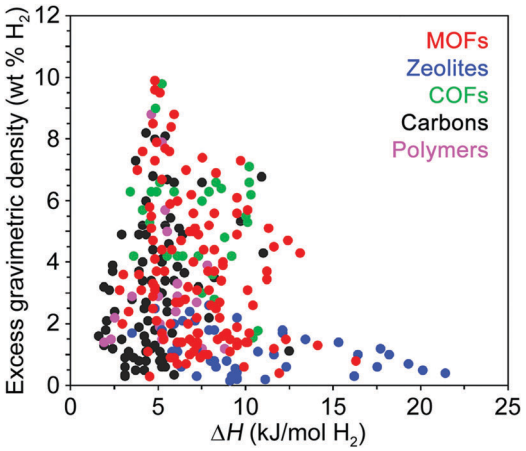

Fig. 4 Excess gravimetric H_2 uptake *versus* enthalpy of H_2 adsorption for various classes of hydrogen storage materials. The adsorption enthalpy values were taken from ref. 26 and 30–33 and are reported at cryogenic conditions, typically between 77 and 87 K.

in Fig. 4, and this data reveals that maximum gravimetric uptake at cryogenic temperatures tends to correlate with H_2 adsorption enthalpies near 5 kJ mol^{-1}.[26,30–33] Qualitatively, a similar trend is observed for volumetric capacities as a function of adsorption enthalpy, although this comparison is difficult as volumetric capacities can be determined in different ways (*e.g.*, utilizing the bulk *vs.* packing density of a material), resulting in substantially different values.

A few studies have noted that adsorption enthalpies in the range of 15–25 kJ mol^{-1} H_2—corresponding to H_2-framework interactions intermediate between strong physisorption and weak chemisorption—are optimal targets for reversible hydrogen storage.[25,34,35] It is important to highlight that these analyses assume a system operating at near-ambient conditions, and adsorption enthalpies are intimately tied to system storage temperatures. Generally speaking, materials with higher heats of adsorption are more likely to exhibit impressive room temperature hydrogen storage behavior. However, because these materials can exhibit steep capacity increases at low pressures, very high heats of adsorption can actually lower usable capacity at a given temperature due to a large amount of inaccessible H_2 that remains adsorbed below 5 bar. As the isotherm slope increases, usable capacity will eventually begin to decrease, therefore requiring an upper limit on targeted heat of adsorption values. This balance between high heat of adsorption and optimal usable H_2 capacity must be considered when comparing classes of storage materials.

Camp and Haranczyk recently investigated the impact of temperature and binding energy on adsorbent usable capacity, and the results of this study are reported here for the first time. The analysis focused on a model material with the same structure as M_2(dobdc) (M-MOF-74 or CPO-27-M; M = Mg, Mn, Fe, Co, Ni, Cu, or Zn; dobdc^{4-} = 2,5-dioxido-1,4-benzenedicarboxylate), which contains the highest density of open metal sites of any known framework. The adsorption energy of H_2 in M_2(dobdc) was modeled by mixing Lennard-Jones parameters for each atom in the structure with Lennard-Jones parameters for hydrogen atoms.

For example, the adsorption energy between a framework Mg^{2+} site and an adsorbed H_2 molecule was calculated by using values of σ_{H_2} = 2.958 Å and ε_{H_2} = 36.7 K[36] and σ_{Mg} = 2.961 Å and ε_{Mg} = 55.895 K[37] in the Lorentz–Berthelot mixing rule[38] and applying the 12-6 Lennard-Jones equation:

$$U_{ij} = 4\varepsilon_{ij}\left[\left(\frac{\sigma_{ij}}{r_{ij}}\right)^{12} - \left(\frac{\sigma_{ij}}{r_{ij}}\right)^{6}\right] \quad (1)$$

In this model system, the H_2-open metal site interaction energy was artificially altered by varying the ε parameter for each metal from 0 to 2×10^4 K, yielding interaction energies of 0–163 kJ mol^{-1}. This variation allowed for the simulation of hypothetical binding interactions with H_2 heats of adsorption (at low coverage) as high as 16 kJ mol^{-1}. As a means of probing the effect of strong binding site density, an additional variable corresponding to the fraction of active open metal sites was introduced. This approach was realized by assigning a portion of the total metal sites a dummy value of ε = 0 K, effectively making them inactive for H_2 binding. Each pixel on the heat map plots in Fig. 5 corresponds to the output of an independent Grand Canonical Monte Carlo (GCMC) simulation at a given active open metal site concentration (*x*-axis) and open metal site interaction strength (*y*-axis).

These simulations showed that at cryogenic temperatures (77 K, Fig. 5b), open metal sites with high interaction energies are not needed to maximize H_2 usable capacity, because the enhancement these sites provide results in a large percentage of the adsorbed H_2 binding at very low pressures. Thus, a considerable portion of the H_2 remains bound to the material in the discharged state at 5 bar and therefore cannot be utilized as fuel. At near-ambient temperatures (243 K, Fig. 5d), stronger and more open metal sites are desired to increase usable capacity, because isotherms are much flatter in the low-pressure region and less H_2 is bound to the material in the discharged state. At intermediate temperatures (180 K, Fig. 5c), there is an interesting interplay between these effects—materials that have fewer open metal sites display fairly constant usable capacities regardless of the binding strength at those sites, and materials with more open metal sites display higher usable capacities as the binding strength at those sites decreases.

This work demonstrates that estimating system-level performance is more complicated than simply targeting materials with binding strengths within a specific range, highlighting that the proposed 15–25 kJ mol^{-1} target enthalpy range for adsorbent materials is only applicable to a certain set of storage conditions at ambient temperatures. We note that this study was carried out for gravimetric capacity only and that as a similar study on volumetric capacity would be valuable. An ideal study would combine, in some form, the two types of sensitivity analyses described in this section, investigating the effect of optimizing both pore structure and strong binding sites.

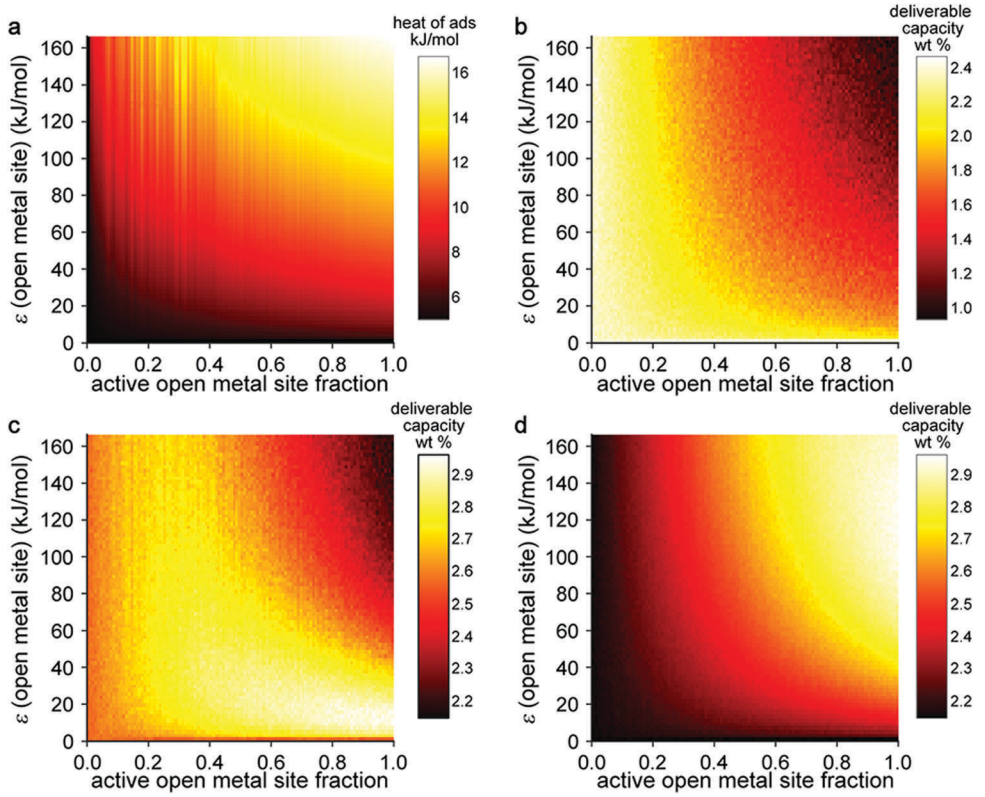

Fig. 5 Results of a GCMC study investigating the effect of active open metal site fraction and Lennard-Jones ε parameter on the H_2 capacity of a model system based on the Mg_2(dobdc) structure type. (a) Heat of adsorption for H_2 at low loading; usable capacity at (b) 77 K; (c) 180 K; and (d) 243 K given a pressure swing between 100 and 5 bar.

We expect that further development of high throughput simulation approaches and material databases (including both real and hypothetical structures) will enable such analyses. Machine learning techniques will likely play a role in simplifying resulting data into practical materials design rules.

Finally, we note that the entropy change upon H_2 adsorption can also influence the overall adsorption thermodynamics, and the magnitude of this value is dominated by the loss of the hydrogen gas entropy in the form of translational, vibrational, and rotational degrees of freedom.[35,39,40] However, it is believed that ΔH has a greater effect on the overall thermodynamics of hydrogen adsorption in adsorbents. As a general rule, increasing the strength of the interaction between the H_2 molecule and the storage material—except for a few special cases and conditions, such as when this increase results in decreased deliverable capacities—appears to enhance overall material performance, and a major thrust of current materials development efforts are focused on strategies to optimize this interaction.

Theoretical calculations of H_2 physisorption

Theory has proven to be an invaluable tool for predicting promising new target storage materials, their properties (*e.g.*, adsorption isotherms), and for interpreting experimental data. In this section, we provide an overview of key computational methods and a qualitative sense of their strengths and weaknesses. Understanding the limitations and relative accuracy of various theoretical methods is important for experimentalists assessing the likelihood that a materials strategy predicted theoretically will be successful. Some of the most common theoretical methods used to compute H_2 interactions with adsorbent materials are presented in Table 3, along with the relative strengths and limitations of each method. The methods are divided into three categories, each of which is summarized below.

Introduction to theoretical methods

The first category in Table 3 includes various static total-energy methods based on first principles that are generally used to evaluate accurate H_2 binding energies, as well as certain enthalpy and entropy contributions. These simulations are run at 0 K, and their primary advantages are relative accuracy and transferability (*i.e.*, general applicability), because they rely on quantum mechanics and can therefore capture a variety of physical contributions in an unbiased way, including dispersion, hybridization, and charge transfer. Typically, these methods are used to compute specific interactions between H_2 molecules and individual sites, which makes them suitable for computing quantities such as ΔH in the low-pressure regime, where interactions between H_2 molecules can often be ignored. Examples of such approaches include *ab initio* wavefunction methods commonly associated with quantum chemistry,[41–43] Quantum Monte Carlo (QMC),[44–46] and density functional theory (DFT).[47–50] Each method offers different strengths in computational accuracy, expense, and model complexity.

The second category consists of dynamical methods, which have the advantage of providing explicit properties at finite temperatures, including enthalpy contributions from gas–gas interactions, as well as vibrational, rotational, and translational entropy contributions. This treatment provides specific advantages for accurately computing the entropy of systems with intermediate-strength binding, for which the available degrees of freedom cannot otherwise be readily approximated. Approaches include *ab initio* molecular dynamics based on DFT[51–53] and classical molecular dynamics based on empirical force fields.[54]

The third category of computational approaches includes statistical–mechanical methods for computing equilibrium thermodynamics—most notably, GCMC simulations.[54–58] These simulations use a stochastic Monte Carlo approach that varies the number of H_2 molecules as well as their positions. This strategy permits evaluation of thermodynamic equilibrium properties at any constant H_2 pressure. The advantages of GCMC make it the most widely used technique for evaluating full H_2 adsorption isotherms, the results of which can be directly compared with experimental data. Because GCMC simulations generate many individual configurations, the corresponding energies are usually evaluated with empirical force fields for computational efficiency.

In the following sections, we explore some of the challenges in accurately predicting H_2 physisorption using several of the abovementioned techniques, including key sources of error. We also provide an overview of current trends in the development of improved methods and offer recommendations for best practices, including acceptable concessions when choosing between computational efficiency and accuracy.

Binding energy predictions

Density functional theory approaches and improvements in density functionals. Density functional theory[47–50] is the predominant electronic structure method for modeling gas interactions with complex systems because it offers a favorable trade-off between binding energy accuracy and computational cost. The exchange–correlation (XC) contribution to the energy is the only parameter that cannot be evaluated exactly and instead must be treated by XC density functional approximations. Starting roughly 12 years ago, researchers began to augment these functionals with damped atom–atom potentials that describe dispersion (so-called $-D$ corrections) in order to reproduce proper binding curves for noncovalent interactions.[77–82] Indeed, no existing functional that excludes dispersion can be recommended for predicting accurate physisorption binding energies. For H_2 physisorption, these dispersion-corrected DFT functionals were able to yield the first near-quantitative agreement with experimental binding energies.[68,69] Although their sophistication continues to advance, $-D$ corrections are not necessarily the best-founded DFT approaches to H_2 binding calculations.[70,83,84] Today, the most accurate and physically meaningful DFT methods for non-bonded interactions are derived from functionals that include nonlocal density–density correlations.[70] The root-mean-square errors of molecular interaction energies from some widely used functionals across a

Table 3 Common theoretical approaches for computing the properties of H_2 physisorption in adsorbent materials

	Method	Key properties determined	Typical accessible scales	Benefits	Limitations and challenges	Sample references
Static first principles	*Ab initio* wavefunction methods (quantum chemistry)	Binding energies, vibrational frequencies within static approximation	50–100 atoms, depending on method	High accuracy (especially CCSD(T)), including explicit evaluation of correlation	Very high computational expense; limited to finite cluster models; no dynamical information; limited scalability on modern architectures	41–43 and 59–61
	Quantum Monte Carlo (QMC)	Binding energies	~100 atoms	High accuracy, including explicit evaluation of correlation; provides systematic statistical measure of convergence; can be applied to clusters or extended systems; highly scalable on modern architectures	Very high computational expense; no dynamical information, explicit forces, or structural optimization; requires geometry inputs from DFT or experiments	44–46 and 62–67
	Static density functional theory (DFT) with van der Waals corrections	Binding energies, vibrational frequencies within static approximation	~1000 atoms	Generally offers best overall tradeoff between accuracy and computational expense; can be applied to clusters or extended systems	Intermediate computational expense; accuracy is dependent on choice of XC functional, which is not always straightforward	47–50 and 68–70
Dynamical	*Ab initio* molecular dynamics (AIMD)	Dynamic vibrational frequencies; entropy; enthalpy contributions from gas–gas interactions	Hundreds of atoms (<100 ps)	Based on DFT, so it accounts for polarization, hybridization, charge transfer, *etc.* within dynamics; explicitly captures anharmonic contributions to entropy; can include relaxation of sorbent geometry	Intermediate to high computational expense; short time scales complicate convergence of statistical quantities; difficult to simulate large frameworks or amorphous systems; no quantum nuclear effects; usually requires fixing total H_2 molecules; inherits same limitations as DFT	51–53
	Classical molecular dynamics and empirical force-field methods	Adsorption enthalpy; entropy; enthalpy contributions from gas–gas interactions	Millions of atoms (depends on complexity of force field; ~1 ns)	Can access much longer scales than first-principles methods; low computational expense for robust convergence of thermodynamic quantities; can include quantum nuclear effects approximately; can include relaxation of sorbent geometry (with properly parameterized potentials)	Parameterization and accuracy validation are difficult; poor transferability; can fail to capture physics of stronger-binding interactions and anharmonicity; usually requires fixing total H_2 molecules	57 and 71–74
Statistical mechanical	Grand Canonical Monte Carlo (GCMC)	Full pressure–temperature–composition equilibria; adsorption isotherms	Determined by method for energy computation (usually similar to classical MD)	Robust statistical–mechanical method allows for calculation of composition-dependent equilibria; allows for variation of total H_2 molecules; typically uses empirical force fields for accessing long scales	Accuracy and limitations depend on method for computing interaction energy (usually empirical force fields); no dynamical information; vibrational/rotational/translational entropy must be computed separately; most implementations assume fixed sorbent geometry	56–58, 75 and 76

large database of 1744 benchmark computed non-bonded interactions are shown in Table 4.[48] It is evident that the width of the distribution of errors roughly reduces by a factor of two from the standard $-D$ corrections to the best available methods.

Nevertheless, although improving quantitative accuracy remains the goal of DFT XC functional development, it is worth emphasizing that qualitative trends in binding energy are often reproduced even with comparatively simple functionals, including generalized gradient approximations (GGAs) with standard $-D$ corrections. Indeed, most modern dispersion-corrected DFT methods (such as those in Table 4) tend to give consistent trends for binding that are derived almost exclusively from dispersion forces. For adsorbent materials that feature significant H_2 interactions beyond dispersion, as is generally the case for the most promising hydrogen storage materials, the results can be more varied. While permanent electrostatic effects are typically adequately described even by the simplest DFT XC functionals, treatment of more complex contributions such as Lewis acid–base interactions and backbonding, which involve charge transfer, induction, and orbital hybridization,[59,60] can differ broadly across functionals (see Fig. 6 for an example). In these latter cases, predicted trends should be treated with a degree of caution unless the most sophisticated XC functionals are employed, since individual physical contributions may be treated at different levels of accuracy. As a general rule, the safest approach when evaluating the reliability of a predicted binding trend is to limit comparisons to systems

Table 4 Root-mean-square (RMS) error-based ranking of 10 widely-used DFT functionals based on analysis of 200 total functionals against a database of 1744 intermolecular interaction energies from highest-accuracy quantum-chemical reference calculations[48]

Rank	Functional	RMS error (kJ mol^{-1})
1	ωB97M-V	0.75
2	B97M-rV	0.91
3	ωB97X-V	0.99
4	B97M-V	0.99
5	B3LYP-D3(CSO)	1.27
13	BLYP-D3(BJ)	1.42
25	TPSS-D3(CSO)	1.53
62	PBE-D3(CSO)	1.89
115	PBE-D2	2.69
159	PBE	8.19

for which the primary underlying physical interaction is very similar. This allows one to take advantage of intrinsic error cancellation. Notably, there have also been recent efforts to introduce error estimation directly into the formulation of the XC functional.[85]

First-principles approaches beyond DFT accuracy. A few methods exist for performing high-level calculations that guarantee benchmark-level accuracy exceeding that conventionally achieved with DFT (even after dispersion corrections are included). Although these methods are generally too computationally demanding for routine use on larger systems, they provide a useful gauge with which to compare calculations of H_2 binding strengths using lower-level methods. Post-Hartree–Fock wavefunction-based quantum-chemical techniques, such as coupled cluster calculations with singles, doubles, and perturbative triples (CCSD(T)), are often considered the "gold standard".[41–43] However, CCSD(T) and related methods are limited to molecules and small clusters that are not representative of the full complexity of most adsorbents. Accordingly, such methods are best employed as benchmarks for other theoretical techniques, and a degree of caution is recommended when comparing the results directly to experimental Q_{st} measurements.

Quantum Monte Carlo (QMC) is an alternative benchmark method for modeling noncovalent interactions that affords similar accuracy to CCSD(T) and yet can be applied equally to molecular clusters or to extended periodic systems.[44–46] To date, most QMC calculations of H_2 physisorption have focused on molecular clusters, including Ca^{2+} complexes,[62,63] certain metal–organic complexes,[64,67] and aromatic carbon complexes.[65,66] The results of these calculations can vary significantly from DFT with simple XC functionals; for instance, in the case of Ca^{2+}, QMC predicted that the binding of four H_2 molecules is energetically unstable or hardly stable (and then only at 0 K),[62,63] in contrast with earlier DFT and MP2 calculations that predicted stable binding of up to eight H_2 molecules.[86,87] Likewise, Fig. 6 shows substantial discrepancies between QMC binding energies of H_2 on Cu_2(bptc) (MOF-505; bptc^{4-} = 3,3′,5,5′-biphenyltetracarboxylate) and a number of DFT-based results; such analyses can aid selection of the best DFT XC functionals. An important qualification for QMC is that input geometries must be precisely known (*e.g.*, from neutron diffraction) or obtained using DFT or another lower level of theory.

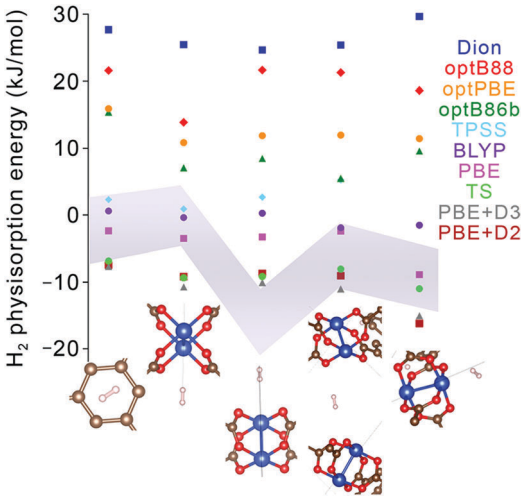

Fig. 6 Hydrogen physisorption energies (colored data points) at different binding sites in Cu_2(bptc) (MOF-505) predicted using lower-level GGA DFT functionals (PBE, BLYP) and several different formulations of van der Waals-corrected and meta-GGA DFT functionals (Dion, optB88, optBPE, optB86b, TPSS, TS, PBE+D2, PBE+D3).[68,79,88–91] Results are compared with the one-σ (68%) confidence interval obtained from QMC runs (grey shaded region). Geometries for each of the sites (bottom) were fixed to those obtained from PBE+D3 and exhibit little variation with the chosen method, unlike the binding energies. The systematic statistical nature of QMC allows for downselecting appropriate DFT functionals for different types of binding sites, with confidence levels based on the degree of QMC convergence.

Approaches based on empirical force fields. Standard force field forms, such as the universal force field (UFF), Dreiding, and OPLS-AA, are appropriate for evaluating the competition between dispersion and Pauli repulsions that control the interaction of H_2 with weak-binding sites, such as uncharged organic linkers in MOFs.[37,92,93] However, stronger H_2 bonding interactions involving open metal sites and/or charged ions, where permanent electrostatics, induction, and charge transfer enhance the binding strength and invalidate generic force field forms, instead necessitate system-specific parameters. One example showing the critical role of electrostatic parameters is the simulation of H_2 binding in a series of M_2(dobdc) materials.[94]

These shortcomings suggest the use of a hybrid approach, in which first-principles-derived binding energies are used to parameterize force fields for the stronger-binding interaction sites (often aided by energy decomposition analysis to isolate individual physical contributions[95–97]), with reliance on more standard force-field formulations for H_2 intermolecular interactions and weaker-binding sites. The development and assessment of system-specific force fields for H_2 binding and release in adsorbents is a topic for a review in itself.[58,98–100] Note that most of the articles referenced here are not specific to H_2, but the successful approaches are generic to the binding of any small, non-polar, closed-shell molecule in a nanoporous framework.

Thermodynamic factors beyond binding energy

As a result of significant improvements in first-principles approaches and increased computing power that can facilitate

larger benchmark calculations, the evaluation of electronic binding energies is no longer necessarily the accuracy-limiting step in computational studies of the binding free energy of H_2. In this subsection, we briefly review other key thermodynamic factors.

Additional contributions to enthalpy of H_2 binding. The conversion of electronic binding energies to binding enthalpies is typically accomplished using the standard rigid rotor (RR)/harmonic oscillator (HO) approximation. However, the main drawback of this approximation is overestimation of the zero point energy (ZPE) due to anharmonicity in the HO model. Although anharmonic effects associated with the H–H stretch mode can be readily treated to improve the ZPE, proper evaluation of the finite-temperature thermal corrections to the enthalpy using quantum chemistry methods requires modification of the RRHO model[101,102] or full solution of a non-local nuclear Schrödinger equation for the soft modes.[103]

Entropy of H_2 binding. The limits of static electronic structure calculations become apparent in evaluating the entropy of H_2 binding. In general, stronger binding limits the available degrees of freedom and will therefore tend to lower the entropy of the gas molecule. However, it can be quite difficult to predict the degree to which the entropy of an H_2 molecule will be reduced upon adsorption. Indeed, the RRHO model for gas-phase entropy is well known to perform poorly, even for the entropy of formation of simple hydrocarbons. The simplest useful alternative is Grimme's free-rotor interpolation approach, which avoids RRHO divergences associated with low frequencies.[101] Although qualitatively superior in difficult cases, the results obtained from this approach cannot be considered quantitative because of the empirically chosen interpolation parameter. A more sophisticated, non-empirical option is to solve one-dimensional Schrödinger equations for each mode. However, it has not yet been established whether this approach can achieve nearly quantitative accuracy for H_2 binding in MOFs in general.[104,105]

Alternatively, entropic contributions can be computed directly from finite-temperature molecular dynamics (either *ab initio* or classical methods). One promising approach for using dynamics trajectories to interpolate and extrapolate entropy over a broad range of temperatures is the two-phase thermodynamic method of Lin *et al.*[106] This method has been used to evaluate the entropy of pure CO_2, as well as adsorbates confined within zeolites, suggesting a similar approach may be adopted to obtain accurate entropies of bound H_2.[107,108]

Nuclear quantum effects. Among the small molecules commonly considered for adsorption applications, H_2 is unique due to the potential relevance of nuclear quantum effects. Thus, special approaches are often required to treat delocalized quantum nuclear motion in H_2. For example, successful simulation of spectroscopic probes of H_2 rotational motion in MOFs and COFs requires explicit solutions of quantum equations for the five relevant degrees of freedom.[109,110] Inclusion of delocalized quantum nuclear motion is likewise critical in order to reliably simulate H_2 binding and obtain uptake curves with quantitative accuracy.[111,112]

The most widely used approach for incorporating nuclear quantum effects is to modify GCMC and classical molecular dynamics *via* a so-called Feynman–Hibbs potential.[113] Reasonably good agreement with experimental results has been obtained for H_2 adsorption in a range of MOF systems using this approach.[14] Another recent example is H_2 adsorption in $Zr_6O_4(OH)_4(bdc)_6$ and $Zr_6O_4(OH)_4(bpdc)_6$ (known as UiO-66 and UiO-67, respectively; bdc^{2-} = 1,4-benzenedicarboxylate, $bpdc^{2-}$ = biphenyl-4,4′-dicarboxylate).[75] Full path-integral formulations of GCMC have also been recently explored.[76]

Adsorbent models

The previous sections focus primarily on efforts to improve the accuracy of predicted H_2 binding thermodynamics. However, another potential source of error arises from the adsorbent models themselves, which are often simplified to render them computationally accessible. Here, we briefly explore some of the primary issues associated with reducing model complexity for both framework materials with long-range order (*e.g.*, MOFs) and high surface-area amorphous materials such as porous carbons.

Framework materials. In the case of periodic framework structures such as MOFs and COFs, model simplifications typically involve the use of cluster geometries to approximate local binding sites. Such approaches have proven successful in many cases, including modeling H_2 binding in $M_3[(M_4Cl)_3(BTT)_8]_2$ (M-BTT; H_3BTT = 1,3,5-tris(tetrazol-5-yl)benzene, M = Cu, Mn, Fe, Zn).[114] However, cluster models neglect the possible influence of effects that extend beyond the immediate vicinity of the H_2 molecule, including electrostatic (Coulomb or dipole) contributions from other sites or functional groups, as well as charge redistribution that may occur across broader regions of the framework. For instance, frameworks in which there is non-local electronic communication from one metal site to another—such as MOF-74, which has quasi one-dimensional metal chains—represent a difficult limit for the cluster approach. Cluster models also neglect to properly address the structural constraints imposed by the extended lattice geometry.

The main alternative to cluster models is the use of periodic boundary conditions (PBCs), which is a natural approach in conjunction with periodic plane-wave basis functions that are commonly used for solid-state DFT calculations.[115] However, these models can be more limited in their accuracy; for instance, while dispersion-corrected GGAs are widely used for PBC-DFT calculations, higher-accuracy functionals are less common due to their high computational cost. It is possible to employ cluster-based corrections to PBC-DFT calculations to achieve greater accuracy in modeling local interactions; examples of their application include H_2 binding in MOF-5 ($Zn_4O(bdc)_3$) and recent work on CO and N_2 binding in Mg-MOF-74.[116,117]

Functionalized carbon and amorphous materials. Highly heterogeneous adsorbents, such as porous disordered carbons and polymers, are extended in nature yet lack specific periodicity. When considering the local interaction of H_2 with defects or functional groups in these materials, the choice between isolated cluster models and extended PBC models depends heavily on the nature of the adsorbent. PBC models are particularly advantageous for two-dimensional materials that are conductive or feature

extended electronic states, such as graphene derivatives. In this case, the electronic and chemical properties of functional groups or defects depend critically on their ability to donate or withdraw charge from a larger conductive reservoir. A striking example of the importance of an extended charge reservoir can be seen in the large differences between the H_2 physisorption energy on graphene and geometrically similar, larger aromatic clusters such as coronene.[66] Models employing periodic boundary conditions are necessary in order to capture this charge reservoir and extended electronic structure. Another factor to consider for materials based on two-dimensional archetypes such as graphene is the possible role of geometric distortions, such as bending, stretching, or folding. These distortions can influence physisorption by altering the chemical properties of the adsorbent over significant distances.[118,119]

In practice, the presence of disorder and heterogeneity can make it impossible to derive an exact model for many adsorbents, particularly within the size constraints of simulation supercells that are accessible to first-principles methods. Instead, a broader picture of the interaction of a material with hydrogen must be derived from simpler representative fragment models. This strategy is best justified if the dominant physical interaction is relatively short-range; examples include interactions with specific functional groups or substitutional defects that introduce polarization and/or partial charge transfer.[120] The actual material may incorporate many different types of functional groups or defects, which can be investigated within the fragment models. However, because this approach does not generate an integrated material model, one cannot utilize GCMC simulations to simulate isotherms over the full pressure range. An alternative is to generate a single representative model based on fragments, provided the computational expense of the larger model can be handled. This hybrid approach has been demonstrated by Singh *et al.*, wherein carbon foam models were constructed by fusing carbon nanotube fragments.[112] These integrated models were then varied systematically and used to examine H_2 adsorption *via* GCMC simulations.

Considerations for adsorbent synthesis and characterization

A lack of reproducibility in the available data on hydrogen adsorption in adsorbent materials has historically proven to be a significant impediment to the field, so much so that the topic was the subject of recent reviews.[5,121,122] Similar concerns have been raised in the context of other adsorbed gases, including CO_2, with new metrics proposed to assess isotherm reproducibility in these systems.[123] Irreproducible and erroneous data span various synthetic, material handling, and characterization methods. With regard to synthetic techniques, the majority of porous frameworks are synthesized solvothermally using common organic solvents, although a diverse set of synthetic strategies is available. These methodologies have been reviewed elsewhere, and the specifics of adsorbent synthesis are not the focus of this section.[124–129] Instead, we present some suggestions for best practices concerning activation and handling of adsorbents as well as characterization methods employed to confirm products and properties, and we also highlight common areas where incorrect approaches lead to inaccuracy in the assessment of candidate adsorbents for H_2 storage.

Adsorbents are not porous until solvent or other pore-templating molecules are removed from the as-synthesized material. This activation process is most simply carried out by heating the material under vacuum, but if this approach is not sufficient, or results in some amount of structural degradation, then more complex solvent exchange methods may be necessary.[130] Materials that contain very large pores, high surface areas, or solvent molecules bound to metal sites in the framework are typically more challenging to activate. Following synthesis, some strongly metal-bound solvent molecules (*e.g.*, *N*,*N*-dimethylformamide [DMF]) can be removed by first performing a solvent exchange, wherein the as-synthesized material is soaked in a lower-boiling or more weakly coordinating solvent (*e.g.*, chloroform or methanol). Over the course of a few days—during which time the soaking solvent is replenished several times—the strongly-bound solvent is gradually displaced and washed from the framework in favor of the soaking solvent. The latter can then be removed from the material by mild heating under vacuum.[29] Drying with supercritical CO_2 drying has become a widespread approach over the last decade, as it has been demonstrated that the negligible surface tension of the carbon dioxide allows for the activation of more delicate structures that otherwise might collapse upon heating. This method is now used commonly by MOF researchers to achieve high surface areas.[131–133]

Regardless of the activation method used, it is of utmost importance to ensure that the extent of activation and chemical composition of the material is known. Activation protocols should be accompanied by combined thermogravimetric analysis and mass spectrometry (TGA-MS) experiments, and routine analysis such as IR spectroscopy can be used to identify stretches arising from solvent molecules, decomposition products, or other impurities. For crystalline materials, powder X-ray diffraction patterns collected before and after activation should be measured to confirm that minimal degradation has occurred. Surface area and pore volume measurements should also be carried out and compared to predictions from crystal structures when possible, to ensure optimum material porosity. Even in rare cases where complete activation of the material is not necessarily desired, a quantitative knowledge of the material composition is still essential to understand adsorption data or cycling ability. Following activation, materials should be handled under inert conditions, regardless of how air- or water-sensitive the samples are, in order to ensure the activated material remains pristine. We note that confirmation that an adsorbent is fully activated is becoming even more critical as synthetic complexity increases, for example for materials targeted to bind more than one H_2 molecule at an individual open metal site.[134] Activation processes for these materials may likely be considerably more difficult than those known to date, and side products or species remaining from metalation reactions or post-synthetic modification will need to be accounted for and completely removed.

Investigation of the adsorption properties of a given material should commence only once diligent activation and characterization procedures have been used to establish that a material is permanently stable, porous, and of known stoichiometry. There are many reviews and documents available to provide guidance on best practices pertaining to hydrogen isotherm collection and data analysis, and the potential errors and difficulties associated with these measurements.[5,135,136] Although improper technique in the measurement of adsorption data can result in inaccurate data, even a properly measured isotherm can be corrupted by a sample that has not been properly activated or handled; unfortunately, in such cases the resulting data do not always appear incorrect or anomalous. Consequently, it is advisable that samples prepared for gas adsorption measurements undergo a degassing step prior to isotherm collection, ideally monitored by mass spectrometry. Desorption and cycling measurements are highly recommended, as these can provide both isotherm quality control and verification of reversibility. A desorption isotherm for a physisorptive material that does not exhibit a large degree of flexibility or a pore-opening mechanism should closely mirror the adsorption isotherm; if it does not, then either an instrumental error, sample degradation, or a side reaction with hydrogen may have occurred.[137] Side reactions can occur in materials with residual reactive groups or surface oxides, resulting in the formation of water or other bound molecules and erroneously high adsorption capacities. However, simple characterization methods can be used post-isotherm collection to check for these reactions.

It is also important to consider sample size when carrying out capacity and other measurements. In general, larger sample size improves the accuracy of isotherm measurements for reasons that are described in detail in the previously referenced best practices document.[135] Often novel adsorbents are prepared using synthetic procedures that yield only small sample sizes, but the suite of high-quality characterization methods described above will typically require gram-scale amounts of adsorbent material to produce the most reliable data. Although increasing material yields beyond a few grams is often secondary to initial exploratory synthesis efforts, it is important to keep in mind that a material that requires difficult or expensive preparation may have diminished utility as a viable storage material. A techno-economic analysis was recently published for three MOFs in the M_2(dobdc) series (M = Ni, Mg, Zn) and provides some valuable insight concerning the aspects of synthetic procedures contributing most to material cost.[138]

Investigations into the nature of hydrogen adsorption beyond storage capacity require additional characterization tools; for example, variable-temperature capacity measurements are commonly used to calculate Q_{st}. Temperature-programmed desorption measurements can also provide information regarding the magnitude of H_2 binding at strong adsorption sites. In addition, *in situ* variable-temperature diffuse reflectance infrared spectroscopy measurements are used to determine the enthalpy of adsorption at a particular binding site.[29,139] For crystalline adsorbents, neutron powder diffraction on deuterium-loaded samples is an extremely powerful technique to elucidate crystallographic binding sites for H_2 molecules.[29,134,140] This method has been extensively used to investigate H_2 bound at open metal sites in MOFs and other strong binding sites, as well as to explain adsorption behavior and direct subsequent synthetic efforts. Inelastic and quasi-elastic neutron scattering techniques can provide further site-specific binding details and insights into H_2 diffusion behavior.[141,142] Finally, although here we are focused on materials challenges, is important to note that it is now possible to predict systems-level performance on the basis of material property data alone, using recently developed models that are continually being updated and are publicly available online for use by researchers.[143]

Revisiting the results of the 2010 HSCoE final report

In 2010, the DOE-funded Hydrogen Sorption Center of Excellence (HSCoE) published a final report recommending that development efforts for specific material classes be continued where viable synthetic routes exist for adsorbents that can potentially meet the DOE onboard storage targets.[4] The four recommended focus areas are summarized below and re-reviewed in light of the previous eight years of advances in the field.

Recommendation 1: develop materials for hydrogen storage by weak-chemisorption *via* a spillover-type mechanism

In so-called spillover materials, H_2 molecules are dissociated at a catalytic site and H atoms are subsequently transferred to high surface-area receptor materials. At the time of the HSCoE study, spillover materials were attractive due to reports that they could exhibit binding energies as high as 10–30 kJ mol^{-1}, and initial analyses suggested that excess gravimetric capacities exceeding 7 wt% should also be possible with such materials.[144–147] Moreover, the center determined that because spillover should be applicable to materials with >1 g mL^{-1} bulk density, storage systems exceeding gravimetric and volumetric capacities of 5.5 wt% and 50 g L^{-1}, respectively, should be achievable at ambient temperature and $\sim$100 bar.

Since then, it has been confirmed theoretically and experimentally that the gravimetric storage limits of materials demonstrating the spillover mechanism are sufficiently low to prevent them from being viable for onboard storage.[148] Investigators have also discovered that effects such as metal oxide reduction of catalyst particles and irreversible hydrogenation reactions plague many spillover materials.[137,149] Many of the previous reports of high capacities in spillover materials ultimately could not be reproduced, leading to an extended debate in the literature concerning several of the assumptions that drove research on these materials around the time of the HSCoE report.[121,150–156] Consequently, spillover materials are no longer a significant focus of hydrogen storage materials research.

Recommendation 2: develop materials for multiple-dihydrogen storage on designated sites

Research aimed at demonstrating binding of multiple H_2 molecules at a single site continues to be a major focus within the hydrogen

storage community. As will be described in subsequent sections, this recommendation presents a daunting synthetic challenge, and only recently has the binding of more than one H_2 molecule at a metal site been experimentally demonstrated.[134] The associated synthetic efforts are being accompanied by development of advanced computational approaches as outlined earlier, which predict that materials of this type have the potential to meet DOE targets.[59]

Recommendation 3: develop substituted/heterogeneous materials with demonstrated hydrogen binding energies in the range of 10–25 kJ mol^{-1}

This recommendation concerns materials such as doped carbons or framework materials with sites that can achieve H_2 binding enthalpies >10 kJ mol^{-1}, with the intention of enabling storage at near-ambient conditions. Efforts to strengthen H_2 binding continue to be important, and broadly speaking, this strategy is probably receiving the greatest attention in the field today; several types of materials currently under investigation in this category are discussed below.

Recommendation 4: limit development of materials in which the storage mechanism is physisorption to only those with optimized structures

This recommendation refers to weakly binding adsorbents, *i.e.*, non-functionalized carbons or MOFs without open metal sites, in which H_2 binds to pore surfaces solely by van der Waals interactions and without enhanced polarization through chemically-functionalized moieties. The report recommends that only materials with surface areas >3000 m^2 g^{-1} and optimized pore sizes in the range of 0.7–1.5 nm should be considered, as these properties are likely necessary to achieve uptakes approaching the DOE targets. Research aimed at synthesizing structures with optimized or well-controlled features is ongoing and benefits from modeling and structural database screening (described above, with data shown in Table 2 and Fig. 3) that correlates uptake with specific crystallographic features.[13,14] Of course, these materials may require cryogenic or low-temperature operation and will therefore need to exhibit extremely high volumetric capacities to be viable for application.

Perspectives on current material strategies

In the sections below, we briefly review recent work on several classes of adsorbents that have either been extensively evaluated for H_2 storage or are currently under evaluation. Their strengths and weaknesses are discussed alongside existing challenges impeding progress. The literature review is not intended to be comprehensive, but rather illustrative of our assessment of progress and potential for the material strategies embodied in each of these classes.

MOFs containing metals with unsaturated coordination spheres

In stable inorganic molecular complexes, the coordination sphere of a metal ion is typically fully occupied with organic ligands and/or anions, and the removal of even weakly-bound coordinated species may lead to collapse of the structure or generation of a reactive species prone to decomposition. The metal sites of as-synthesized MOFs are also typically coordinated with organic linkers, solvents such as DMF and ethanol, and/or counter anions such as OH^- and F^-; however, the rigidity of these frameworks often renders it possible to remove such molecules (*via* heating or exposure to vacuum, or some combination) without loss of structural integrity. Importantly, the resulting exposed framework metal coordination sites can exhibit strong Lewis acidity, making the material advantageous for gas capture applications.[157,158] The accessibility of open metal sites within a MOF was first shown for Cu_2(ATC) (also known as MOF-11; ATC^{4-} = adamantane-1,3,5,7-tetracarboxylate), wherein removal of coordinated water molecules from the Cu^{2+} sites could be accomplished without loss of framework crystallinity or surface area.[159] The absence of water within the structure was confirmed by single crystal X-ray diffraction studies. Shortly after the first study of H_2 adsorption in MOF-5, the framework MOF-505, which also exhibits open Cu^{2+} coordination sites, was investigated for H_2 adsorption.[160,161] Upon removal of coordinated water and/or acetone molecules, the fully desolvated material exhibited an increased H_2 uptake (2.41 wt% *versus* 1.39 wt%) at 77 K and 1 bar.

As mentioned previously, detailed characterization of H_2 adsorption at framework open metal sites can in some cases be afforded by techniques such as *in situ* neutron diffraction and diffuse reflectance infrared spectroscopy. In 2006, low temperature neutron diffraction studies of Mn-BTT revealed that H_2 adsorption primarily occurs at the exposed Mn^{2+} sites of the square planar Mn_4Cl units (Fig. 7).[140] The distance between Mn and D_2 determined from these measurements (2.27 Å) was much shorter than observed previously between D_2 and the saturated $Zn_4O(CO_2)_6$ cluster of MOF-5 ($\sim$3.1 Å).[162] Strong binding due to polarization of the H_2 molecule was supported by a distinctive downshift of the adsorbed H_2 stretching band (4038 cm^{-1}) compared to that in MOF-5 (4128 cm^{-1}), observed by *in situ* IR spectroscopy.[114,163] The IR absorption band at 4038 cm^{-1} evolved gradually as the temperature was lowered from 150 to 14 K, with two peaks arising at 4126 and 4133 cm^{-1} (below 100 K) and a third absorption band appearing at 4140 cm^{-1} (below 40 K). Here, the band at 4038 cm^{-1} corresponds to the adsorption of H_2 at the Mn^{2+} sites and, importantly, the temperature dependence of this peak can provide a means of determining the thermodynamic parameters for adsorption at these specific sites.[29,114] From the van't Hoff plot, the magnitude of the ΔH value for the primary binding sites in Mn-BTT was estimated to be -11.9 ± 0.6 kJ mol^{-1}, which is slightly greater than the Q_{st} for Mn-BTT (-10.1 kJ mol^{-1}), extracted from low-pressure H_2 adsorption measurements.[114,140] Note that such differences are typical since the Q_{st} values are averaged over all adsorbed H_2 species.

Owing to their high concentration of coordinatively-unsaturated metal sites, the M_2(dobdc) family of frameworks (M = Mg, Co, Ni, Mn, Fe, and Zn) have also been heavily explored for H_2 storage (Fig. 7). In this structure type, M^{2+} ions are connected through 2,5-dioxido-1,4-benzene-dicarboxylate linkers to form one-dimensional

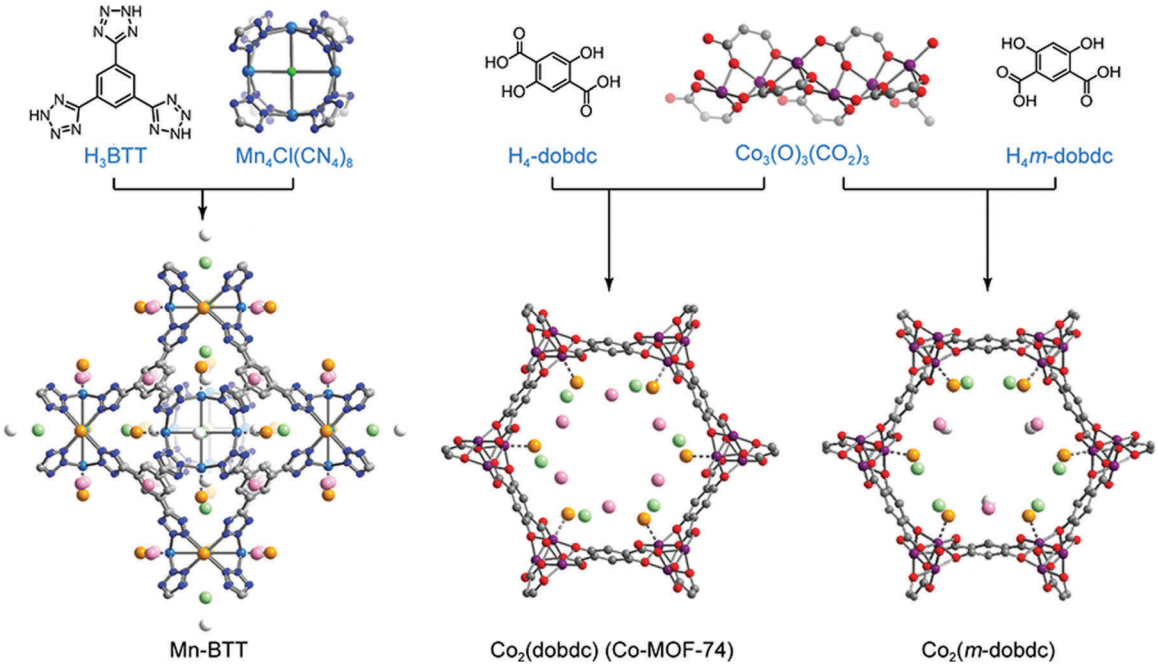

Fig. 7 (top) Molecular structures of organic linkers and inorganic building units comprising the Mn-BTT, Co_2(dobdc), and Co_2(*m*-dobdc) MOFs. (bottom) Crystal structures of each framework loaded with D_2 (16 molecules per Mn_4Cl unit in Mn-BTT and 2.25 D_2 per Co^{2+} for Co_2(dobdc) and Co_2(*m*-dobdc)). Gray, red, dark blue, blue, and purple spheres represent C, O, N, Mn, and Co atoms, respectively. Deuterium molecules adsorbed at primary, secondary, ternary, and quaternary sites are shown in large orange, light green, pink, and white spheres, respectively. D_2-framework interactions for the primary binding site are drawn as dotted lines. Hydrogen atoms of organic linkers are omitted to clarify.[29,140]

hexagonal channels that extend along the *c*-axis of the crystal, and the octahedral coordination environment of each metal in the as-synthesized material is completed by a solvent molecule. This solvent is readily removed with heating under vacuum to yield one-dimensional channels replete with open metal sites. Hydrogen adsorption has been extensively investigated in this series[29,164–166] and it has been shown that at low pressures the strength of the metal–H_2 interaction is highly dependent on the identity of the framework metal ion. From H_2 isotherm measurements, the Q_{st} value for Ni_2(dobdc) was estimated to be -11.9 kJ mol^{-1},[29] and across the entire series the $-Q_{st}$ values follow the trend $Zn^{2+} < Mn^{2+} < Fe^{2+} < Mg^{2+} < Co^{2+} < Ni^{2+}$. This trend in the metal–H_2 interaction strength generally follows the Irving–Williams series for high spin octahedral transition metal complexes, such that the $-Q_{st}$ values increase as metal ion radius decreases.[167]

More recently, the structural isomer of M_2(dobdc), M_2(*m*-dobdc) (*m*-dobdc^{4-} = 4,6-dioxido-1,3-benzenedicarboxylate, M = Mg, Mn, Fe, Co, Ni) (Fig. 7), was identified as a promising alternative material for H_2 adsorption, due to the greater charge density of its open metal sites and the lower cost of the organic linker.[29] Interestingly, although the porosity of the M_2(*m*-dobdc) series is similar to that of M_2(dobdc), the former materials exhibit higher H_2 uptake at 77 K and 1 bar, associated with $-Q_{st}$ values that are larger by 0.4–1.5 kJ mol^{-1} when comparing metal congeners. For example, the Q_{st} value for Ni_2(*m*-dobdc) was estimated from low-pressure H_2 isotherms to be as large as -12.3 kJ mol^{-1}, compared to a slightly smaller magnitude of -11.9 kJ mol^{-1} for Ni_2(dobdc). While the significance of this difference could be debatable in the absence of error, values of ΔH for the Ni–H_2 interaction in Ni_2(*m*-dobdc) and Ni_2(dobdc) were estimated from *in situ* IR spectroscopy to be -13.7 and -12.3 kJ mol^{-1}, respectively, supporting a much stronger H_2 interaction in the former material. Rigorous comparison of M_2(*m*-dobdc) and M_2(dobdc) materials *via* neutron diffraction, IR spectroscopy, and electronic structure calculations revealed that a subtle difference in the local metal environment leads to an increased positive charge density at the open metal sites of the M_2(*m*-dobdc) compounds, promoting greater charge transfer from H_2 to the metal center and leading to an enhanced metal–H_2 interaction energy.[29] Neutron diffraction characterization of Ni_2(*m*-dobdc) also revealed tight packing of adsorbed D_2 and a short $D_2\cdots D_2$ contact of 2.82 Å between molecules adsorbed at primary and secondary sites (Fig. 7). This distance is even smaller than the distance of 3.23 Å observed between molecules in solid H_2 at 5 K and highlights the potential for strong primary binding sites to promote a significant increase in the density of adsorbed H_2 within the entire pore structure.[168] These favorable H_2–Ni^{2+} interactions and resulting efficient confinement of H_2/D_2 within the pores of Ni_2(*m*-dobdc) result in this framework exhibiting the highest storage capacity to date for an adsorbent operating at 298 K and pressures up to 100 bar. Notably, when used in a process with temperature swings between -75 and 25 °C, this material achieves a usable volumetric capacity of 23.0 g L^{-1} in the pressure range of 5–100 bar.[169]

Metal cation exchange reactions have also been explored with MOFs as a means of tuning their gas adsorption properties, including the enhancement of the magnitude of Q_{st}.[170]

These exchange reactions can also be a useful way to prepare new framework structures, especially if direct synthesis and activation of a particular materials proves challenging.[171,172] In relation to H_2 storage, a simple strategy was proposed and demonstrated in 2007 to improve the H_2 adsorption properties of the framework Mn-BTT.[173] In this work, metal cation exchange of the Mn-BTT structure resulted in successful isolation of the frameworks $M_3[(Mn_4Cl)_3(BTT)_8]_2$ (M = Li^+, Cu^+, Fe^{2+}, Co^{2+}, Ni^{2+}, Cu^{2+}, Zn^{2+}). The surface area of the series of metal-exchanged materials was slightly lower than the parent Mn-BTT structure, although a slightly larger Q_{st} value was observed for $Co_3[(Mn_4Cl)_3(BTT)_8]_2$ compared to $Mn_3[(Mn_4Cl)_3(BTT)_8]_2$ (−10.5 *versus* −10.1 kJ mol^{-1}, respectively). Based on the computational study of the aluminosilicate zeolite ZSM-5, it has also been proposed that Cu^+-exchanged materials can exhibit strong H_2 binding, although it was not possible to prepare a Cu^+-rich M-BTT material.[173,174] In 2014, Cu^+ sites were introduced into the MFU-4*l*-type material $Zn_5Cl_4(BTDD)_3$ (H_2BTDD = bis(1*H*-1,2,3-triazolo[4,5-*b*],[4′,5′-*i*])dibenzo[1,4]dioxin) by a three-step, post-synthetic reaction, and the structure of the resulting material, Cu(I)-MFU-4l, was determined by X-ray diffraction.[175] In this procedure, two Cu^{2+} ions in the metalated $Cu(II)_2Zn_3Cl_4$ cluster were treated with lithium formate to yield Cu(II)-MFU-4*l*-formate $[Cu(II)_2Zn_3Cl_2(BTDD)_3(formate)_2]$, which was heated under vacuum to yield exposed Cu(I) sites. Hydrogen isotherm measurements revealed a 1 : 1 binding of H_2 to the Cu(I) sites (corresponding to an uptake of 0.34 wt%) over the temperature range of 163–193 K, and 80% of the metal sites were found to be occupied by H_2, even at 273 K and 1 bar. From H_2 adsorption measurements, the Q_{st} value for Cu(I)-MFU-4*l* was estimated to be −32.3 kJ mol^{-1}, which, to our knowledge, is the highest value reported to date for any MOF. We note that the strength of this interaction in this framework may in part arise due to back-donation of electrons from the Cu metal center to H_2, as has been observed in Kubas-type complexes (see below). Although this binding strength falls beyond the target range of −15 to −25 kJ mol^{-1} considered to be optimal for ambient-temperature H_2 storage with a maximum pressure of 100 bar,[25,35] targeting materials that possess metal ions capable of such back-donation and simultaneously exhibit strong physisorption may be a promising strategy to enhance storage capacity.

As materials are further developed to meet the current DOE onboard hydrogen storage targets (Table 1), one challenge that remains is to increase the density of strong binding sites, such as open metal sites, within a given volume of framework space. It is possible that strategies such as engineering frameworks with shorter organic linkers and optimizing pore topology will promote progress toward this goal, but most likely new material concepts and synthetic chemistry will be necessary to meet the targets.[176] For example, prior to being synthesized in the lab, promising novel or already known materials for post-synthetic metalation reactions could first be identified using computational screening tools as outlined in the section on usable gravimetric and volumetric capacities. This type of targeted synthesis could result in materials with strong binding sites within pore structures that also demonstrate efficient H_2 packing.

Binding of multiple H_2 molecules to an open metal site in a MOF or other material

The hydrogen storage capacity of a MOF is to some extent dictated by the H_2 binding enthalpy, but a high initial $-Q_{st}$ value does not necessarily guarantee a high storage capacity, because in most frameworks each metal site is capable of binding only a single H_2 molecule.[29] For example, in a framework such as Ni_2(*m*-dobdc) that exhibits an open metal site density of ∼6 mmol g^{-1}, binding of one H_2 per metal site would achieve a storage density that is only one quarter of the 2020 DOE target of 23.5 mmol g^{-1} (= 4.5 wt% H_2). Considering that metal centers are not the exclusive adsorption sites for gas molecules within a framework, the design of materials exhibiting a high affinity for H_2 and metal centers capable of binding more than one H_2 molecule may drastically improve storage capacity.[29,166] In this section we introduce two representative classes of materials that may be promising in this regard, namely molecular metal complexes and extended frameworks capable of reversibly binding multiple H_2 molecules per metal center. We also briefly discuss possible future research directions in this area.

Kubas compounds. In the early 1980s, certain molecular metal complexes, now known as Kubas complexes, were observed to reversibly bind one or more H_2 molecules.[177,178] The first example of a Kubas complex was $W(CO)_3(PiPr_3)_2(\eta^2\text{-}H_2)$, a yellow solid synthesized by exposing the five-coordinate, 16-electron precursor $W(CO)_3(PiPr_3)_2$ to an H_2-rich atmosphere (Fig. 8).[179] Interestingly, in the presence of an Ar atmosphere or under vacuum, this yellow solid undergoes an immediate color change to dark purple, the color of the precursor complex, indicating that H_2 binding and liberation is fully reversible. The coordination environment of the η^2-bound H_2 molecule within $W(CO)_3(PiPr_3)_2(\eta^2\text{-}H_2)$ was studied *via* single-crystal neutron diffraction, which revealed an H–H bond distance of 0.84 Å. This distance is longer than the 0.74 Å distance between atoms in free H_2, indicating that the interaction between the H_2 molecule and the metal center is stronger than simple physisorption, a conclusion that was also supported by ^{1}H NMR and IR spectroscopic data.[180] The unexpected H_2 bonding interaction was attributed to the back-donation of electrons from the metal to H_2, in addition to σ-bond

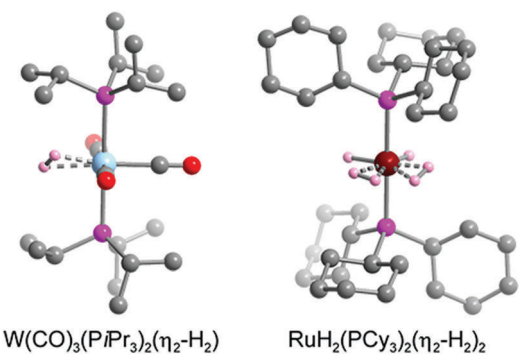

Fig. 8 Crystal structure of $W(CO)_3(PiPr_3)_2(\eta^2\text{-}H_2)$ (left) and $RuH_2(PCy_3)_2(\eta^2\text{-}H_2)_2$ (right).[179,182] Gray, red, pink, blue, dark red, and light pink spheres represent C, O, P, W, Ru, and coordinated H atoms, respectively. Hydrogen atoms of the triphosphine ligands are omitted for clarity.

formation. Notably, expected H_2 binding energies for Kubas complexes can reach values as high as 80 kJ mol^{-1} as a result of the strength of this back-donation.[60] However, the enthalpy of H_2 addition to another Kubas complex, $W(CO)_3(PCy_3)_2$ (Cy = cyclohexyl), was estimated to be only 45 kJ mol^{-1} by calorimetric measurements, due to favorable agostic C–H interactions between metal and phosphine ligand.[181]

While the first Kubas complexes exhibited only a single side-on bound H_2 ligand, later metal complexes were identified that could reversibly bind two H_2 molecules without cleaving the H–H bond.[182–185] One representative example is the complex $RuH_2(PCy_3)_2(\eta^2\text{-}H_2)_2$, the structure of which was elucidated by single-crystal X-ray diffraction (Fig. 8).[182,183] In this complex the two bulky phosphine ligands are located *trans* to each other, similar to the Kubas complexes, although an equatorial coordination pocket results that is capable of binding two H_2 molecules and two hydrides. The H–H bond distance of each η^2-bound H_2 was estimated to be 0.85 Å, a value that is again indicative of a strong interaction when compared to materials exhibiting more conventional H_2 physisorption. As expected given this strong interaction, the Ru–H_2(centroid) distance of ~1.50–1.55 Å is significantly shorter than the metal–D_2 distance of >2.2 Å determined for Ni_2(*m*-dobdc) from neutron diffraction measurements.[29]

Despite binding two H_2 molecules per metal, $RuH_2(PCy_3)_2(\eta^2\text{-}H_2)_2$ only coordinates 0.6 wt% H_2. Alternatively, the incorporation of a dense array of Kubas-type metal centers within a MOF—*e.g.*, low-spin, first-row transition metals such as Cr or Mn[186,187] coordinated by phosphine-based linkers—might be a promising strategy for achieving high H_2 uptake; such a pursuit would no doubt be aided by computational screening of candidate framework structures. While the strength of the M–H_2 bond dissociation energy in such compounds could reduce material usable capacity and cyclability, it is possible that designing Kubas-type sites within a flexible frameworks could offset this effect.

MOFs containing low-coordinate open metal sites. It is well-known that metal centers of as-synthesized frameworks often bind multiple solvent molecules (for example, Mg_3(naphthalenedicarboxylate)$_3$(*N*,*N*-diethylformamide)$_4$).[188] Although the coordinated solvent can persist in the pores even after evacuation, thereby reducing the accessible surface area, the successful removal of the solvent without sacrificing the framework structural integrity could introduce the possibility of binding multiple H_2 molecules per metal center. This strategy was recently employed for the first time using the framework $Mn_2(dsbdc)(DMF)_2$ ($dsbdc^{4-}$ = 2,5-disulfido-1,4-benzenedicarboxylate), first isolated in 2013 (Fig. 9).[189] In contrast to Mn_2(dobdc), the $Mn_2(dsbdc)(DMF)_2$ framework exhibits two crystallographically-independent octahedral Mn^{2+} centers alternating along its one-dimensional hexagonal channels, one of which is fully coordinated by $dsbdc^{4-}$ linkers while the other has its coordination sphere completed by two DMF molecules. Removal of the two *cis*-coordinated solvent molecules results in a stable, activated structure, Mn_2(dsbdc), wherein the previously solvated Mn^{2+} adopts a four-coordinate seesaw geometry.[134] Notably, neutron diffraction measurements carried out at 10 K on a sample of Mn_2(dsbdc) loaded with 0.7 equivalents of D_2 per four-coordinate Mn^{2+} afforded the first example of the binding of two D_2 molecules at a single metal site in a MOF. The observed Mn–D_2 distances (3.40 and 3.07 Å for 0.7 and 1.4 D_2 loadings, respectively) are larger than those measured for the frameworks discussed above, perhaps due to the concave geometry of desolvated Mn^{2+} site, leading to only a moderate initial Q_{st} value of −5.6 kJ mol^{-1}. It is possible that metal exchange reactions with Mn_2(dsbdc) could lead to materials exhibiting an increase in H_2 binding energy and/or the number of adsorbed H_2 molecules.

The framework Zn_2(dobdc) (UTSA-74a) is another material exhibiting two accessible binding sites that was recently studied for C_2H_2/CO_2 separations.[190] The as-synthesized, solvated framework exhibits a binuclear secondary building unit consisting of tetrahedral and octahedral Zn^{2+} ions. The coordination sphere of

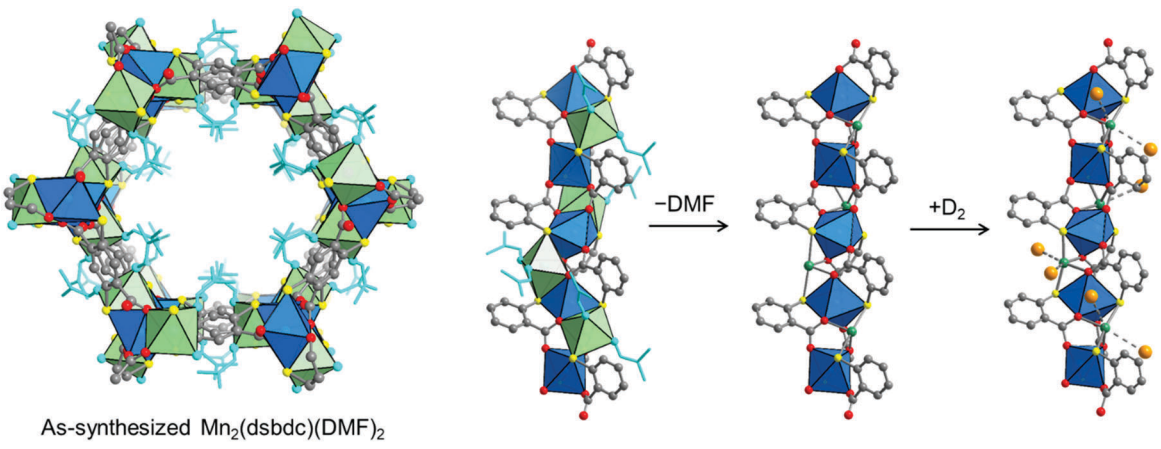

Fig. 9 (left) Crystal structure of $Mn_2(dsbdc)(DMF)_2$.[189] (right) Coordinated DMF molecules (light blue) are removed to create exposed Mn^{2+} centers (green spheres), which adsorb two D_2 molecules at a loading of 0.7 D_2 per four-coordinate Mn^{2+} (at 10 K). Gray, red, yellow spheres represent C, O, and S atoms, respectively; H atoms are omitted for clarity. The coordination spheres of each Mn center are shown as blue and green polyhedra and D_2 molecules are represented by orange spheres.[134]

the octahedral Zn^{2+} is completed by two *trans* water molecules, which can be removed to yield a slightly distorted ZnO_4 unit as observed by single crystal X-ray diffraction analysis. In the same study, DFT calculations predicted that the ZnO_4 unit can accommodate two C_2H_2 adsorption sites at high loadings, a result that may have wider implications for the binding of other gases, including H_2.

These recent reports afford valuable insight for continued optimization of framework design, although precise control over the inorganic unit remains a challenge. One alternative strategy for accessing open metal sites is to design ligands exhibiting secondary coordination sites that can be selectively metalated following framework synthesis.[191] When compared with the direct synthesis of frameworks using pre-metalated linkers (*e.g.*, metalated porphyrin or salen linkers),[192–194] post-synthetic metalation is also potentially advantageous for accessing a wide variety of chelating moieties and metal ion combinations, although it is important to note that in some cases the protection of chelating sites is required during initial framework synthesis. One of the earliest examples of a framework prepared *via* post-synthetic metalation was reported in 2005, wherein the 1,1′-bi-2-naphthol moiety of the framework $CdCl_2$(DCDPBN) (DCDPBN = 6,6′-dichloro-4,4′-di(pyridin-4-yl)-[1,1′-binaphthalene]-2,2′-diol) was metalated with titanium isopropoxide.[195] Following this report, additional frameworks exhibiting 2,2′-bipyridine and salicylate sites were successfully metalated, and some of the resulting materials exhibited enhanced gas adsorption properties compared with the bare parent frameworks.[196,197] However, metalation of neutral chelating groups resulted in pore-confinement of the counter anions and consequently diminished porosity and reduced accessibility of H_2 to the metal center.

Another approach is to utilize organic linkers with catecholate sites, which can offer charge-balance for post-synthetically chelated divalent metal ions and obviate the need for countercations that would diminish porosity and capacity. The successful synthesis and subsequent metalation of a framework with catechol groups was first reported in 2010 by Tanabe *et al.*[198] In this work, the authors prepared the framework $Zn_4O((OBnNO_2)_2\text{-}BDC)(BTB)_{4/3}$ (or nitrobenzyl-protected UMCM-1, $(OBnNO_2)_2$-BDC^{2-} = 2,3-bis((2-nitrobenzyl)oxy)-1,4-benzenedicarboxylate, BTB^{3-} = 4,4′,4″-benzene-1,3,5-triyl-tribenzoate),[199] which exhibits nitrobenzyl-protected BDC linkers. The nitrobenzyl groups could be removed by irradiation with 365 nm light, and the resulting catechol-functionalized UMCM-1 was then reacted with an iron(III) acetylacetonate solution to impregnate the framework with Fe^{3+} metal ions. Similar reactions have been carried out using Cr^{3+} and V^{4+} salts, which demonstrate the wide applicably of post-synthetic metalation reactions.[200,201] These latter metalated frameworks were studied only for their utility in oxidative catalysis, however, and thus further efforts are necessary to examine the H_2 affinity of metal-catecholate sites.

The interaction of H_2 with some metal-catecholate clusters has been predicted computationally, and it was found that the H_2 adsorption enthalpy exceeds that of metal-biphenol or metal–bipyridine complexes.[59,60] For example, it was calculated that Mg^{2+} and Ca^{2+} catecholate complexes would exhibit H_2 adsorption energies of 23.0 and 15.1 kJ mol^{-1}, respectively, compared to the differential adsorption energies ΔE = 4.7 and 5.5 kJ mol^{-1} for biphenyl-(TiO_4)-Me_2 and bipyridine-$CuCl_2$.[60] The significant enhancement of the adsorption enthalpy can be attributed to the strong dipole moment created by the negatively charged oxygen atoms and positively charged metal ion—in other words, a local polarization interaction is critical to increase the binding energy of H_2. It should be noted that the predicted M–H_2 interaction energies for the Mg^{2+} and Ca^{2+} catecholate complexes are much lower than the H_2 binding enthalpies determined for Kubas complexes ($\sim$80 kJ mol^{-1}) because of the absence of back-bonding from the alkaline-earth metal ions to H_2, and these values are within a more optimal range for ambient temperature H_2 storage. Importantly, within a UiO-66-type structure, it was predicted that Ca^{2+}–catecholates are able to bind up to four H_2 molecules per metal site without significant differences between the successive adsorption energies, resulting in a high calculated H_2 volumetric usable capacity of 30 g L^{-1} at 298 K (pressures ranging from 5.8–100 bar).[59] Therefore, the development of successful experimental protocols for the metalation of catechol-based frameworks (including the successful desolvation of any coordinated solvents) should be a key target for synthetic chemists.

Porous organic frameworks

In principle, the gravimetric storage capacity of H_2 within a given framework could also be improved if the transition metal nodes were replaced with lighter atoms, such as carbon and nitrogen, without sacrificing the robustness of the framework. To synthesize such organic polymers, multitopic organic molecular building blocks are assembled into multidimensional structures *via* a metal-catalyzed (*e.g.*, Pd or Ni) coupling reaction.[202,203] Due to their strong covalent linkages, the resulting polymer frameworks generally exhibit high stability and, importantly, can exhibit permanent porosity in the absence of crystallinity, in contrast to MOFs. Porous organic polymers can be divided into several subclasses, based on the linkage and aromaticity of the organic framework, although we will not consider these differences here.[203]

A major advance in the chemistry of porous organic polymers came in 2009 with the discovery of high hydrothermal stability and exceptional surface area in the material PAF-1 (PAF = porous aromatic framework), a robust framework synthesized *via* a homo-coupling reaction with the tetrahedral building block tetrakis(4-bromophenyl)methane (Fig. 10).[204] This material exhibits a high BET surface area of 5600 m^2 g^{-1} (Langmuir surface area = 7100 m^2 g^{-1}) and excess gravimetric H_2 uptake of 7.0 wt% at 77 K and 48 bar. Shortly after this report, several isoreticular organic frameworks were synthesized using larger tetrahedral building blocks.[205,206] Among these materials, the framework known as PPN-4 (assembled using the tetrakis(4-bromophenyl)silane building unit) was found to possess a remarkably high BET surface area of 6461 m^2 g^{-1} (Langmuir surface area = 10 063 m^2 g^{-1}) and excess H_2 adsorption as high as 8.3 wt% at 77 K and 55 bar.[206] Porous organic frameworks can also be accessed using tritopic and tetratopic building blocks, as was demonstrated with the isolation of the framework JUC-Z7,

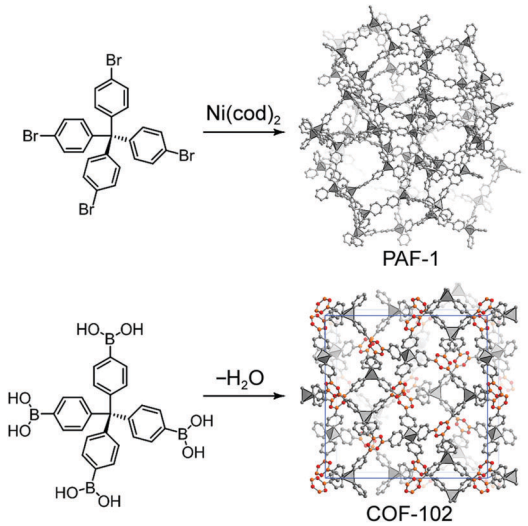

Fig. 10 Schematic representation of the synthesis of PAF-1 (top) and COF-102 (bottom).[204,208] Gray, red, and orange spheres represent C, O, and B atoms, respectively; quaternary carbon atoms are shown as grey tetrahedra and H atoms of the triphosphine ligands are omitted for clarity.

assembled from tetrakis(4-bromophenyl)methane and tris(4-bromophenyl)amine. This material also exhibits high porosity, with a BET surface area of 4889 $m^2\ g^{-1}$ and excess gravimetric H_2 uptake of 6.4 wt% at 77 K and 48 bar ($-Q_{st}$ = 5.6 kJ mol^{-1}).[207] It should be noted that, similar to other high surface area materials mentioned previously, these materials do not exhibit high volumetric storage capacities due to their very large pores.

At least two challenges must be addressed to improve the H_2 storage capacity in porous organic frameworks. The first challenge is the generally low experimental surface areas (typically $<1500\ m^2\ g^{-1}$) exhibited by porous organic frameworks, relative to expected values, especially for those materials exhibiting additional functionality. The formation of an interpenetrated structure is one likely source of low porosity, which can result from π–π interactions between neighboring frameworks and/or monomeric building blocks.[209,210] Recent theoretical studies suggest these π–π interactions can be mitigated by replacing monomer phenyl and alkyne groups with rigid alkyl groups, while introducing bulky side chains into the framework structures may additionally increase the probability of forming dense frameworks.[211] In the same work it was also proposed that interpenetrating structures could be avoided by the use of bulky coupling catalysts with dimensions similar to the target framework pore diameter.

A second challenge inherent in using porous organic frameworks for H_2 storage is that these materials are only weakly polarizing and thus do not strongly bind H_2. As discussed above in the context of MOFs, post-synthetic metalation of porous organic frameworks is one possible strategy for improving H_2 binding energy. Successful pre- and post-synthetic metalation reactions have been demonstrated for a limited numbers of porous organic polymers exhibiting bipyridine, salen, porphyrin, and catechol chelating moieties.[212–215] For instance, Weston *et al.* prepared catechol-functionalized porous polymers that could be cleanly metalated with $MgMe_2$, $Cu(CH_3CO_2)_2$, or $Mn(CH_3CO_2)_2$, as demonstrated using IR spectroscopy.[215] Metalation with Mn^{2+} afforded a material that exhibited an increase in Q_{st} relative to the parent framework (−9.6 and −8.1 kJ mol^{-1}, respectively), although it was not clear if this enhancement was directly related to the metalation. Fischer *et al.* have alternatively demonstrated that an anionic framework can be utilized to immobilize metal cations, through successful synthesis of a Li^+-decorated borate-based porous polymer *via* coupling of lithium tetrakis(tetrafluorophenyl)borate and triethynylbenzene.[216] The resulting material was found to exhibit moderate porosity, with a surface area of 890 $m^2\ g^{-1}$ that was retained upon exchange of Li^+ with Na^+ or Mn^{2+} cations (surface areas of 731 and 499 $m^2\ g^{-1}$, respectively). Future work would benefit from the investigation of the relationship between metal ion coordination environment and H_2 adsorption in such materials.

Covalent organic frameworks

It is possible to achieve crystallinity in porous organic frameworks through the reversible reaction of monomeric organic building blocks *via* condensation reactions of 1,4-benzenediboronic acid and hexahydroxytriphenylene.[217] This class of crystalline materials, known as covalent organic frameworks (COFs), now encompasses two-dimensional layered structures and three-dimensional frameworks with various linkages such as B–O, C–N, B–N, and B–O–Si.[217–221] Two-dimensional layered COFs are primarily composed of either hexagonal or square layers, which are stacked in an eclipsed fashion and can be tuned by changing the dimensions of the organic monomers to yield varying pore diameters.[222] Three-dimensional COFs are often synthesized by linking tetratopic (tetrahedral and square) building units with linear or triangular organic units, although the first such material was prepared by the self-condensation reaction of tetra(4-dihydroxyborylphenyl)methane (Fig. 10).[208] Because the topology of these materials is dependent on the directionality of the organic building blocks, the range of reported structures is limited relative to MOFs. Typical three-dimensional topologies (or nets) are diamond, carbon nitride, boracite, and platinum sulfide, and similar to their amorphous analogues, these materials are also prone to form interpenetrated structures.[208,219,223]

Covalent organic frameworks are generally thermally and structurally robust, and activated samples can therefore be prepared without loss of crystallinity. The surface areas of activated COFs have been evaluated by both N_2 and Ar adsorption analysis, and the reported values vary widely depending on the framework structure. For example, the two-dimensional materials COF-6 (prepared from the condensation reaction of hexahydroxytriphenylene and 1,3,5-benzenetriboronic acid) and CTF-1 (prepared from the condensation reaction of 1,4-dicyanobenzene) were found to exhibit BET surface areas of 750 and 791 $m^2\ g^{-1}$, respectively, whereas the BET surface areas for three-dimensional frameworks COF-102 and COF-103 (prepared from the self-condensation reactions of tetra(4-(dihydroxy)borylphenyl)methane and tetra(4-(dihydroxy)borylphenyl)silane, respectively), were calculated to be 3620 and 3530 $m^2\ g^{-1}$.[208,220,224,225] As expected, COF-102 and

COF-103 exhibit high excess gravimetric H_2 uptakes (6.8 and 6.6 wt%, respectively) at ~35 bar and 77 K, although their initial Q_{st} values are only −3.9 and −4.4 kJ mol^{-1}, respectively, due to a lack of strong H_2 binding sites.[225] Two-dimensional COFs such as COF-10 (prepared from the condensation reaction of hexahydroxytriphenylene and 1,4-benzenediboronic acid) and BLP-2(H) (obtained from the thermal decomposition of 1,3,5-(*p*-aminophenyl)benzene-borane) have been found to exhibit rather moderate saturation excess uptakes of 3.8 and 2.5 wt% at 77 K, relative to three-dimensional variants and the porous polymers described above.[221,225] Importantly, the Q_{st} values for two-dimensional COFs with similar pore diameter do not appear to be drastically influenced by the identity of linking moieties. For instance, changing from boronate (COF-6) to borazine (BLP-2(H)) to azine (ACOF-1; prepared by a condensation reaction of hydrazine hydrate and 1,3,5-triformylbenzene) resulted in frameworks with Q_{st} values of −7.0 kJ mol^{-1}, −6.8 kJ mol^{-1}, and −6.0 kJ mol^{-1}, respectively.[221,225,226] The similarity of these values may be due in part to the fact that only the edge of each two-dimensional layer is exposed for interactions with H_2 molecules, and suggests that such COFs are not ideal materials for practical H_2 storage.

Although the impregnation of covalent organic frameworks with metal ions or metal particles could in principle lead to enhanced H_2 storage capacities, this area of synthetic research has not been widely explored. To date, frameworks have been constructed with metalloporphyrin linkers or doped with $Pd(CH_3CO_2)_2$, molybdenyl acetylacetonate, or various metallocenes.[227–231] In one of the latter examples, COF-102 was impregnated with $Pd(\eta^3\text{-}C_3H_5)(\eta^5\text{-}C_5H_5)$ and then photodecomposed to yield Pd nanoparticles in the pores. The H_2 uptake of the resulting material Pd@COF-102 was found to be slightly lower than that of pristine COF-102 at 77 K; at 298 K and 20 bar, however, the H_2 uptake was 2.6 times greater than the pristine sample (0.42 compared to 0.16 wt%, respectively) due to the additional chemisorption of H_2 on Pd.[231] While frameworks doped with $Pd(CH_3CO_2)_2$ and molybdenyl acetylacetonate were investigated for applications in catalysis, H_2 adsorption characterization was not reported for any frameworks other than Pd@COF-102. We note that the presence of electron-deficient metal sites in these materials, arising from the electron withdrawing nature of the coordinated groups, could be of relevance for future study in pursuit of materials for H_2 storage.

Graphene and graphene oxide materials

Since its discovery, graphene has been explored as a next-generation material for H_2 storage with the view that its single-carbon atomic sheet could offer an ideal lightweight adsorbent with a vast, open structure. However, due to the weak enthalpic interaction between graphene and H_2 molecules, use of graphene as an adsorbent requires cryogenic temperatures that, as discussed above, increase the cost and complexity of the fueling system.[232] Over the last few decades, synthetic research has led to development of new graphene-inspired building blocks and several new carbon-based H_2 adsorbents designed to enhance binding enthalpies,

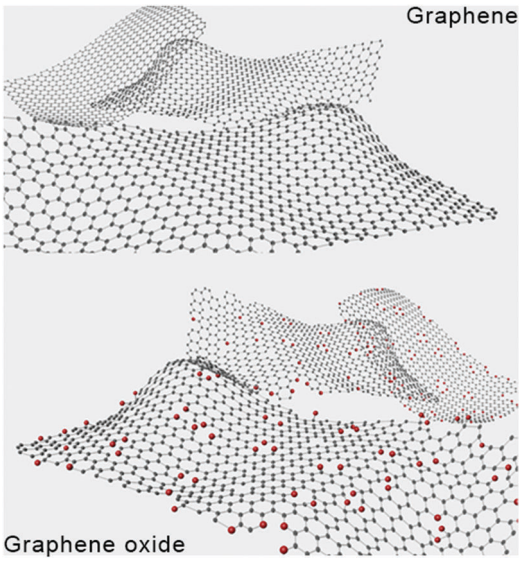

Fig. 11 Schematic illustration of single-atom layer graphene and graphene oxide.

such as graphene oxide, graphene origami, and others.[233–235] For example, various oxygenated functional moieties, including carboxyl and hydroxyl groups, can be introduced to graphene to form graphene oxide (Fig. 11); subsequent crosslinking of this scaffold with organic ligands can be carried out to prepare three-dimensional H_2 adsorbents. Burress *et al.* reported the preparation of a layered graphene oxide structure of this type by reacting varying amounts of benzene-1,4-diboronic acid with graphene oxide sheets.[235] GCMC simulations predicted an optimum interlayer separations of 1.1 nm and an ideal carbon atom-to-boronic acid ratio of 32 : 1 for balancing structural stability with layer accessibility and H_2 adsorption capacity. They successfully synthesized a material with roughly these properties which displayed an uptake of 1 wt% at 77 K and 1 bar with a Q_{st} value of 9 kJ mol^{-1}, comparable to some MOFs.

More recently, Klechikov *et al.* evaluated the H_2 adsorption properties of various graphene and graphene oxide materials prepared *via* rapid thermal exfoliation and post-exfoliation activation treatments, which enabled them to systematically study the dependence of H_2 uptake *versus* surface area.[236] The authors found that H_2 uptake by graphene materials does not exceed 1 wt% at 120 bar H_2 at ambient temperatures; however, uptake at 77 K increases linearly as a function of material surface area, and a maximal H_2 uptake of ~5 wt% was observed for a graphene with a surface area of 2300 m^2 g^{-1} (roughly following Chahine's rule behavior).[10] The authors concluded that bulk graphene samples follow the standard H_2 uptake trends of other nanostructured carbons and do not demonstrate intrinsically superior capacities; thus, unmodified graphene-based materials are essentially weakly-binding adsorbents.

Recently, Kim *et al.* studied the H_2 adsorption properties of aggregated mesoporous graphene oxide intercalated with potassium ions, with the goal of demonstrating experimentally—in two dimensions—the thermodynamic principle that the density of H_2 in a potential well increases exponentially relative to the

ambient gas by the corresponding Boltzmann factor.[234] The authors reported a gravimetric H_2 storage density of 4.65 wt% at 40 bar and room temperature for this material, although in the absence of potassium ions they found the material exhibits a storage density of 0.21 wt% at $\sim$5 bar. The exceptional H_2 uptake was rationalized as arising from the attractive potential of the mesopores and the intercalated potassium ions and, if accurate, would be the highest value reported for any adsorbent at ambient temperature; however validation of this result is needed by means of more comprehensive isotherm measurements on bulk samples beyond the quartz-crystal microbalance method used in the study. Further characterization of these materials should also be carried out to rule out the type of undesired side reactions that result in erroneously high capacities described above for materials containing surface oxides or reactive groups.

The malleable nature of graphene offers another potentially valuable route for the preparation of high-capacity H_2 adsorbents, for example, Zhu and Li have proposed a hydrogenation-assisted graphene origami for hydrogen storage.[233] Using MD simulations, the authors showed that a origami nanocage—which can be converted between open or closed configurations *via* an external electric field—could obtain a gravimetric capacity up to 9.7 wt%. Such a concept, although interesting, has yet to be experimentally verified.

A few experimental and theoretical studies have recently reported that enhanced H_2 uptake can be achieved by metal atom doping of graphene surfaces. For example, Beheshti *et al.* predicted that double-sided Ca-decorated graphene doped with 12 atomic% of individual boron atoms can theoretically achieve a gravimetric H_2 capacity of 8.38 wt% with an average binding energy of $\sim$38.6 kJ mol^{-1}.[237] Lee *et al.* similarly reported a first-principles study on hydrogen adsorption over Ca-decorated zigzag graphene nanoribbons (ZGNR), which predicted that each Ca atom is capable of binding up to six H_2 molecules at a binding energy of $\sim$19.3 kJ mol^{-1} of H_2, leading to a H_2 gravimetric capacity of $\sim$5 wt%.[87] However, both studies employed a relatively low level of DFT, which, as discussed above, is not always consistent with higher levels of theory (*e.g.*, QMC calculations), and so these values should perhaps be interpreted with caution. Moreover, the synthesis of such adsorbents with low-coordinate dopant metal atoms that can accommodate several H_2 molecules is likely to be extremely difficult, and has yet to be demonstrated. Nevertheless, some metal-doped carbons have been shown experimentally to exhibit improved storage properties; for example, Chen *et al.* synthesized a Pd-doped two-dimensional graphene sheet mixed with an activated carbon receptor and experimentally found a 49% enhancement in H_2 gravimetric capacity and a higher Q_{st} compared to the undoped mixtures at ambient temperature.[238] In contrast to metal-site H_2 adsorption predicted by the above theoretical studies, these enhancements were attributed to spillover effects. Zhou *et al.* have also reported a Ni–graphene composite containing nanocrystalline nickel particles uniformly dispersed over a graphene substrate, which exhibited room temperature gravimetric H_2 capacities of 0.14 wt% at 1 bar and 1.18 wt% at 60 bar, respectively.[239]

Other graphene derivatives of interest involve new topologies such as carbon nanotubes and porous aromatic sp^2 frameworks. Since the work by Dillon *et al.*, which reported excellent H_2 uptake by carbon nanotubes, extensive research has been conducted on hydrogen storage applications using carbon materials such as nanotubes and graphene derivatives.[240] Despite initial enthusiasm, however, the reported performance by carbon nanotubes has been challenging to reproduce and architectures composed of undoped nanotubes are not a promising class of materials for practical storage applications.[241] On the other hand, with the emerging aforementioned porous materials, other types of three-dimensional graphene architectures have been developed for H_2 storage. Although various approaches to meeting the large storage capacity demands under ambient conditions have been proposed, the weak interactions between graphene materials and H_2 molecules remain a daunting hurdle. Synthetic challenges surrounding metal doping of these structures still exist, including imparting precise control over the species present upon metal insertion, the degree of metal doping, and reversibility of H_2 adsorption at these sites. Regardless, these materials display some potential towards ultimately meeting DOE targets if such challenges can be overcome.

Boron- and other heteroatom-doped carbons

In addition to the graphene and metal-doped graphene materials, there has been considerable effort focused on doping carbon structures with various heteroatoms to increase the H_2 binding enthalpy. A computational study suggested that doping C_{36} fullerenes with boron could lead to an H_2 binding enthalpy of $\sim$20 kJ mol^{-1}, as a result of partial charge transfer from the H_2 σ bond to the localized empty p_z orbital of boron.[65] This level of theory predicted a B–H_2 distance of $\sim$1.4 Å—23% longer than the sum of the covalent radii of B and H (1.14 Å)—and an elongated H–H bond of 0.85 Å that is $\sim$10% longer than the typical molecular distance of 0.77 Å. Fig. 12a illustrates the side-on interaction of H_2 with the sp^2 boron bound in fullerene. It was noted by the authors that the predicted H_2 bond elongation and B–H_2 distance is comparable to the H_2 interaction with metal centers in Kubas complexes (*vide supra*).[184,242] Stable gas phase fullerene compounds containing as many as 12 boron atoms were predicted to be accessible with additional doping.

As a consequence of these promising theoretical studies, a number of experimental approaches have been explored to synthesize boron doped carbon materials with high surface areas and tunable porosity. In one of the first studies, B- and N-doped microporous carbons were synthesized *via* substitution reactions.[243] The resulting doped graphite sheets were found to exhibit much higher surface areas and 53% higher H_2 storage capacity than the pure carbon materials at room temperature. However, subsequent investigations of similar materials found little enhancement of H_2 binding energy or storage capacity. This discrepancy between the computational predictions and the experimental observations is likely due to the difficulty of achieving experimentally the same boron environment that is modeled in the calculations; for example, the boron atom in the

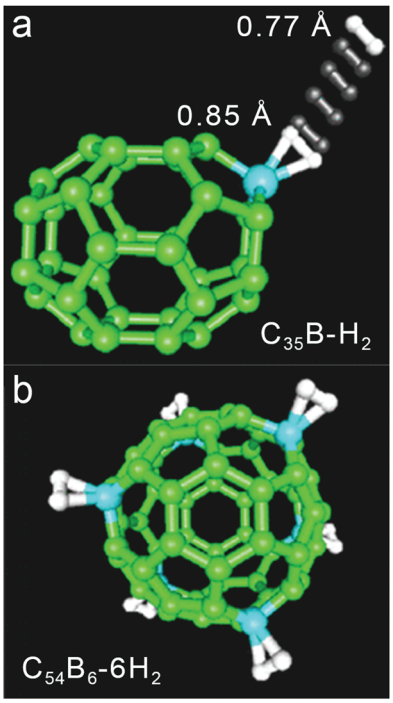

Fig. 12 Structural model illustrating inclusion of one (a) or six (b) boron atoms in a fullerene and their interaction with molecular H_2; green, blue, and white spheres represent C, B, and H atoms, respectively. Reprinted Fig. 1 and 4 (adapted) with permission from Y.-H. Kim, Y. Zhao, A. Williamson, M. J. Heben and S. B. Zhang, *Phys. Rev. Lett.*, 2006, **96**, 016102. Copyright 2016 by the American Physical Society.

above fullerene calculations has a unique BC_3 (sp^2) non-planar, trigonal geometry, it is difficult to realize the same geometry by doping boron into planar graphitic structures. Other early experimental studies attempted to dope carbon with boron using anhydrous boric acid, but this approach provided little control over the doping site or the final functionality. In an attempt to address this synthetic challenge, Chung *et al.* used a specific class of boron-containing polymeric precursors with known connectivity to achieve a controlled approach to incorporating boron.[27] Pyrolysis of the precursors resulted in relatively high surface area carbon materials (780 m^2 g^{-1}) with high boron content (7.2 wt%) and an H_2 binding energy of 11 kJ mol^{-1}. The substitutional p-type boron dopant was proposed to polarize the carbon surface, resulting in a binding energy higher than that achieved with neat carbon but lower than predicted for boron-doped fullerene structures.

The authors further used ^{11}B magic angle spinning (MAS) NMR to gain insight into the boron environment in the carbon framework (Fig. 13).[27] Deconvolution of the spectra of several B-doped carbon materials obtained at different pyrolysis temperatures revealed two components (best illustrated in the pale blue curve in Fig. 13b): one downfield arising from boron sites of trigonal planar symmetry, and one upfield corresponding to boron sites in a puckered configuration (Fig. 13c).

Chung and Jeong subsequently developed an alternative approach to prepare a range of porous boron-doped carbon materials, *via* pyrolysis of polymeric boron precursors in the presence of pore-templating LiCl or NaCl.[244] Annealing at temperatures ranging from 600–1800 °C resulted in a range of structures, from those exhibiting minimal π conjugation and a boron-puckered configuration (600–800 °C) to more ordered structures with extensive π conjugation and a planar configuration (1500 °C). The planar graphitic layers were reported to accommodate <3 mol% B, while the amorphous materials exhibited much higher surface areas (500–800 m^2 g^{-1}) and 12 mol% B. The report claimed experimentally derived binding enthalpies of 12.5 and 20 kJ mol^{-1} for two structures, albeit with low capacities due to the small surface areas of the materials.

Tour and coworkers have alternatively used a bottom-up, solvothermal synthesis approach to prepare boron-, nitrogen-, and phosphorus-doped carbon scaffolds with surface areas as high as 900 m^2 g^{-1}, *via* the reaction of chlorine-containing organic molecules with metallic sodium at reflux in high boiling solvents, followed by the addition of heterotopic electrophiles for dopant incorporation.[245] Hydrogen adsorption data for each material exhibited the expected type I isotherm behavior (Fig. 14), and heats of adsorption extrapolated to zero-coverage afforded Q_{st} values of 8.6 and 8.3 kJ mol^{-1} for boron- and phosphorus-doped carbons, respectively. These values are notably higher than

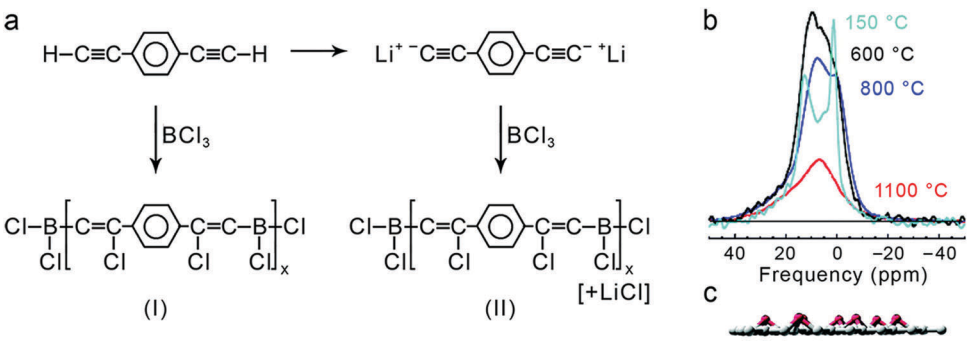

Fig. 13 (a) Synthetic route to boron-containing polymeric precursors used in the synthesis of boron-doped microporous carbons; (b) ^{11}B MAS NMR of materials resulting from pyrolysis of the polymers at 150, 600, 800, and 1100 °C (pale blue, black, dark blue, and red curves, respectively); (c) proposed structure of puckered boron sites obtained at 1100 °C. Adapted with permission from T. C. M. Chung, Y. Jeong, Q. Chen, A. Kleinhammes and Y. Wu, *J. Am. Chem. Soc.*, 2008, **130**, 6668. Copyright 2008 American Chemical Society.

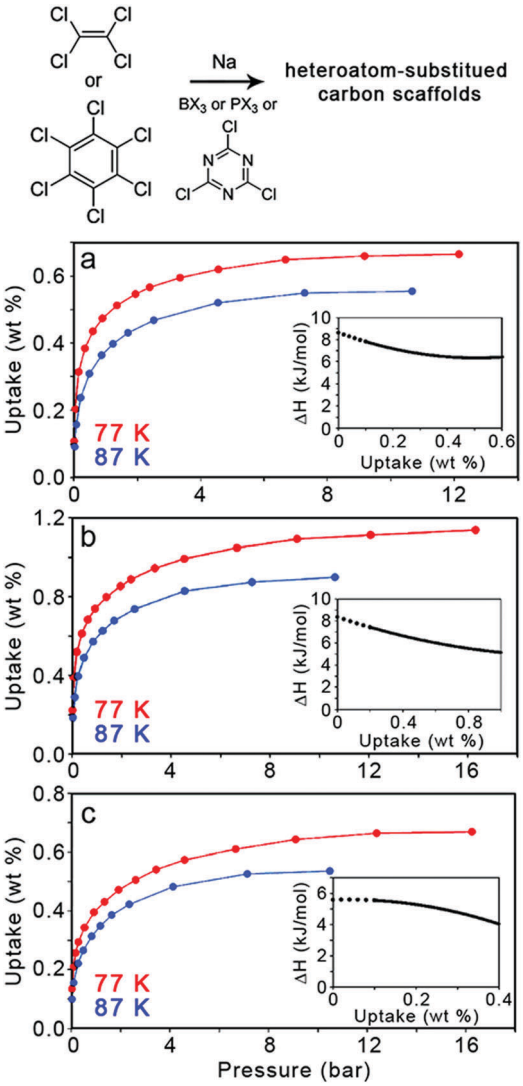

Fig. 14 (top) Bottom-up synthesis of heteroatom-substituted carbons; reaction conditions: tetraglyme, diphenyl ether, or paraffin oil solvent, X = halogen or OR, and temperatures between 250 and 350 °C. (bottom) Hydrogen uptake at 77 and 87 K for (a) boron-, (b) phosphorus-, and (c) nitrogen-substituted carbons. Adapted with permission from Z. Jin, Z. Z. Sun, L. J. Simpson, K. J. O'Neill, P. A. Parilla, Y. Li, N. P. Stadie, C. C. Ahn, C. Kittrell and J. M. Tour, *J. Am. Chem. Soc.*, 2010, **132**, 15246. Copyright 2008 American Chemical Society.

typical binding energies of 4–6 kJ mol^{-1} for undoped carbons, although the nitrogen-doped material was found to have a binding energy of 5.6 kJ mol^{-1}, within this range.

Further experimental and computational work is underway to more precisely quantify the increased enthalpy of adsorption exhibited by these materials as well as to understand how boron modifies the graphitic carbon surface. Trigonal boron is more stable in a planar rather than puckered geometry, as the former enables more efficient electron donation to the electron-deficient boron atom. As such, a defect is generated when boron is substituted into a non-planar carbon matrix, and the nature of this defect may lead to an enhanced H_2 binding energy to the carbon matrix. However, the lack of a reproducible value for the H_2 binding energy in such materials presents a roadblock to their serious inquiry for H_2 storage, and whether the variability in reported values is a reflection of synthetic difficulties or measurement complications remains unclear. Ultimately, any binding energy advantages achieved from boron (or other heteroatom) doping must also be accompanied by the ability to incorporate such sites into carbons with sufficient surface areas and porosities that can accommodate high H_2 capacities.

Conclusions

The recent commercial availability of hydrogen fuel cell electric vehicles represents a major advance for this technology, but the use of compressed gas storage is disadvantageous from a number of perspectives, including insufficient volumetric capacity and the higher costs associated with fueling and infrastructure. Consequently, new solid-state hydrogen storage materials that can meet all of the DOE targets are still a pressing need. Adsorbents are one of two major classes of storage materials currently under consideration for H_2 storage (the other being metal hydrides), and while some of these materials meet many of the DOE targets, one common deficiency is generally low volumetric capacity. Many material strategies have been proposed to address this problem, and some of the most prominent include targeting materials with open metal sites, those that are capable of binding multiple H_2 molecules at a given binding site, and heteroatom-doped carbons. Our intention in this Perspective has been to provide an objective assessment of the strengths, weaknesses, and outstanding challenges for these strategies, both to motivate intensified research and stimulate new efforts in underexplored or completely new areas. Not all strategies discussed here have received in-depth experimental consideration thus far, and some are motivated primarily by predictions from theory. In our estimation, the chosen emphases in this Perspective concerning theoretical methods, synthesis and characterization challenges, metrics of usable gravimetric and volumetric capacities, and trends in binding energies, represent key areas of inquiry in the continued evaluation of materials for ambient temperature H_2 storage. It is our hope that the foregoing discussion will afford interested readers with the requisite background information needed to understand the relevant limitations when evaluating the merits of a particular strategy (new or existing) toward the development and characterization of H_2 adsorbents. For example, theoretical methods used to predict hydrogen uptake vary widely in their accuracy and readers should take this into account in assessing the corresponding predictions. Similarly, synthetic approaches for preparing new storage materials each have their own limitations, and realistic consideration should be given to the difficulties involved prior to embarking on an extensive synthesis campaign. Nevertheless, numerous discoveries and developments in the past decade have created new opportunities to address the challenges facing onboard materials-based storage applications. We are optimistic that successful materials can be found that will meet the requirements for this important transportation technology.

Conflicts of interest

There are no conflicts to declare.

Acknowledgements

The authors thank Jesse Adams for helpful discussions. Sandia National Laboratories is a multi-mission laboratory managed and operated by National Technology and Engineering Solutions of Sandia, LLC, a wholly owned subsidiary of Honeywell International, Inc., for the U.S. Department of Energy's National Nuclear Security Administration (NNSA) under contract DE-NA-0003525. The authors gratefully acknowledge support from the Hydrogen Materials—Advanced Research Consortium (HyMARC), established as part of the Energy Materials Network under the U.S. Department of Energy, Office of Energy Efficiency and Renewable Energy, Fuel Cell Technologies Office, under Contract Number DE-AC04-94AL85000 with Sandia National Laboratories, Contract Number DE-AC36-08-GO28308 with the National Renewable Energy Laboratory, Contract Number DE-AC02-05CH11231 with Lawrence Berkeley National Laboratory, and Contract Number DE-AC52-07NA27344 with Lawrence Livermore National Laboratory. J. U. is supported by the Molecular Foundry at Lawrence Berkeley National Laboratory, which is supported by the Office of Science, Office of Basic Energy Sciences, of the U.S. Department of Energy under Contract Number DE-AC02-05CH11231. Pacific Northwest National Laboratory is a multi-program national laboratory operated by Battelle for the U.S. Department of Energy under Contract Number DE-AC05-76RL01830. Argonne National Laboratory is supported by Office of Science of U. S. Department of Energy under the Contract Number DE-AC02-06CH11357. D. J. S. and A. A. acknowledge financial support provided by the U.S. Department of Energy, Office of Energy Efficiency and Renewable Energy, under Contract Numbers DE-EE0007046 and DE-EE0008093. Partial computing resources were provided by the U.S. National Science Foundation *via* grant 1531752 MRI: Acquisition of Conflux, A Novel Platform for Data-Driven Computational Physics (Tech. Monitor: Ed Walker). Z. H. is supported through the Oak Ridge Institute for Science and Education (ORISE). ORISE is managed by Oak Ridge Associated Universities (ORAU) under DOE Contract Number DE-AC05-06OR23100. The views and opinions of the authors expressed herein do not necessarily state or reflect those of the United States Government or any agency thereof. Neither the United States Government nor any agency thereof, nor any of their employees, makes any warranty, expressed or implied, or assumes any legal liability or responsibility for the accuracy, completeness, nor usefulness of any information, apparatus, product, or process disclosed, or represents that its use would not infringe privately owned rights.

References

1 D. J. Durbin and C. Malardier-Jugroot, *Int. J. Hydrogen Energy*, 2013, **38**, 14595.
2 Target Explanation Document: Onboard Hydrogen Storage for Light-Duty Fuel Cell Vehicles, U.S. Department of Energy, https://energy.gov/sites/prod/files/2017/05/f34/fcto_targets_onboard_hydro_storage_explanation.pdf, accessed Mar 2018.
3 DOE Hydrogen and Fuel Cells Program Record, U.S. Department of Energy, https://www.hydrogen.energy.gov/pdfs/15013_onboard_storage_performance_cost.pdf, accessed Mar 2018.
4 L. Simpson, ''HSCoE Final Report,'' U.S. Department of Energy Fuel Cell Technologies Office, https://www.energy.gov/sites/prod/files/2014/03/f12/hydrogen_sorption_coe_final_report.pdf, accessed Mar 2018.
5 P. A. Parilla, K. Gross, K. Hurst and T. Gennett, *Appl. Phys. A: Mater. Sci. Process.*, 2016, **122**, 201.
6 M. Veenstra, J. Yang, C. Xu, M. Gaab, L. Arnold, U. Muller, D. J. Siegel and Y. Ming, U.S. Department of Energy, Hydrogen and Fuel Cells Program 2014 Annual Merit Review Proceedings: Project ST010, https://www.hydrogen.energy.gov/pdfs/review14/st010_veenstra_2014_o.pdf, accessed Mar 2018.
7 D. L. Anton and T. Motyka, U.S. Department of Energy, U.S. Department of Energy, Hydrogen and Fuel Cells Program 2015 Annual Merit Review Proceedings: Project ST004, https://www.hydrogen.energy.gov/pdfs/review15/st004_anton_2015_o.pdf, accessed Mar 2018.
8 D. P. Broom, C. J. Webb, K. E. Hurst, P. A. Parilla, T. Gennett, C. M. Brown, R. Zacharia, E. Tylianakis, E. Klontzas, G. E. Froudakis, Th. A. Steriotis, P. N. Trikalitis, D. L. Anton, B. Hardy, D. Tamburello, C. Corgnale, B. A. van Hassel, D. Cossement, R. Chahine and M. Hirscher, *Appl. Phys. A: Mater. Sci. Process.*, 2016, **122**, 151.
9 O. K. Farha, A. O. Yazaydin, I. Eryazici, C. D. Malliakas, B. G. Hauser, M. G. Kanatzidis, S. T. Nguyen, R. Q. Snurr and J. T. Hupp, *Nat. Chem.*, 2010, **2**, 944.
10 B. Panella, M. Hirscher and S. Roth, *Carbon*, 2005, **43**, 2209.
11 R. Chahine and P. Bénard, Adsorption Storage of Gaseous Hydrogen at Cryogenic Temperatures, in *Advances in Cryogenic Engineering*, ed. P. Kittel, Plenum Press, New York, 1998, vol. 43, pp. 1257–1264.
12 E. Masika and R. Mokaya, *J. Phys. Chem. C*, 2012, **116**, 25734.
13 J. Goldsmith, A. G. Wong-Foy, M. J. Cafarella and D. J. Siegel, *Chem. Mater.*, 2013, **25**, 3373.
14 A. Ahmed, Y. Liu, J. Purewal, L. D. Tran, A. G. Wong-Foy, M. Veenstra, A. J. Matzger and D. J. Siegel, *Energy Environ. Sci.*, 2017, **10**, 2459.
15 J. A. Mason, M. Veenstra and J. R. Long, *Chem. Sci.*, 2014, **5**, 32.
16 Y. G. Chung, J. Camp, M. Haranczyk, B. J. Sikora, W. Bury, V. Krungleviciute, T. Yildirim, O. K. Farha, D. S. Sholl and R. Q. Snurr, *Chem. Mater.*, 2014, **26**, 6185.
17 R. J. Sadus, *Molecular simulation of fluids: theory, algorithms, and object-orientation*, Elsevier, Amsterdam, 1999.
18 T. L. Hill, *An introduction to statistical thermodynamics*, Dover Publications, 1986.
19 M. Fischer, F. Hoffmann and M. Fröba, *ChemPhysChem*, 2009, **10**, 2647.
20 A. W. Thornton, C. M. Simon, J. Kim, O. Kwon, K. S. Deeg, K. Konstas, S. J. Pas, M. R. Hill, D. A. Winkler, M. Haranczyk and B. Smit, *Chem. Mater.*, 2017, **29**, 2844.

21 D. A. Gómez-Gualdrón, Y. J. Colón, X. Zhang, T. C. Wang, Y.-S. Chen, J. T. Hupp, T. Yildirim, O. K. Farha, J. Zhang and R. Q. Snurr, *Energy Environ. Sci.*, 2016, **9**, 3279.
22 N. S. Bobbitt, J. Chen and R. Q. Snurr, *J. Phys. Chem. C*, 2016, **120**, 27328.
23 D. Gómez-Gualdrón, T. C. Wang, P. García-Holley, R. M. Sawelewa, E. Argueta, R. Q. Snurr, J. T. Hupp, T. Yildirim and O. K. Farha, *ACS Appl. Mater. Interfaces*, 2017, **9**, 33419.
24 Nanoporous Materials Genome Center, http://www1.chem.umn.edu/nmgc/, accessed Mar 2018.
25 S. K. Bhatia and A. L. Myers, *Langmuir*, 2006, **22**, 1688.
26 K. M. Thomas, Hydrogen Adsorption and Storage in Porous Materials, in *Handbook of Hydrogen Energy*, ed. S. A. Sherif, D. Y. Goswami, E. K. Stefanakos and A. Steinfield, CRC Press, 2015.
27 T. C. M. Chung, Y. Jeong, Q. Chen, A. Kleinhammes and Y. Wu, *J. Am. Chem. Soc.*, 2008, **130**, 6668.
28 G. T. Palomino, M. R. L. Carayol and C. O. Arean, *Catal. Today*, 2008, **138**, 249.
29 M. T. Kapelewski, S. J. Geier, M. R. Hudson, D. Stück, J. A. Mason, J. N. Nelson, D. J. Xiao, Z. Hulvey, E. Gilmour, S. A. FitzGerald, M. Head-Gordon, C. M. Brown and J. R. Long, *J. Am. Chem. Soc.*, 2014, **136**, 12119.
30 Hydrogen Storage Materials Database, http://hydrogenmaterialssearch.govtools.us, accessed Mar 2018.
31 S. Tedds, A. Walton, D. P. Broom and D. Book, *Faraday Discuss.*, 2011, **151**, 75.
32 M. P. Suh, H. J. Park, T. K. Prasad and D.-W. Lim, *Chem. Rev.*, 2012, **112**, 782.
33 Y. Xia, Z. Yang and Y. Zhu, *J. Mater. Chem. A*, 2013, **1**, 9365.
34 Y.-S. Bae and R. Q. Snurr, *Microporous Mesoporous Mater.*, 2010, **132**, 300.
35 E. Garrone, B. Bonelli and C. O. Areán, *Chem. Phys. Lett.*, 2008, **456**, 68.
36 V. Buch, *J. Chem. Phys.*, 1994, **100**, 7610.
37 A. K. Rappé, C. J. Casewit, K. S. Colwell, W. A. Goddard III and W. M. Skiff, *J. Am. Chem. Soc.*, 1992, **114**, 10024.
38 H. A. Lorentz, *Ann. Phys.*, 1881, **248**, 127.
39 G. T. Palomino, C. P. Cabello and C. O. Areán, *Eur. J. Inorg. Chem.*, 2011, 1703.
40 S. M. Chavan, O. Zavorotynska, C. Lamberti and S. Bordiga, *Dalton Trans.*, 2013, **42**, 12586.
41 E. G. Hohenstein and C. D. Sherrill, *Wiley Interdiscip. Rev.: Comput. Mol. Sci.*, 2012, **2**, 304.
42 K. E. Riley, M. Pitoňák, P. Jurečka and P. Hobza, *Chem. Rev.*, 2010, **110**, 5023.
43 J. Řezáč and P. Hobza, *Chem. Rev.*, 2016, **116**, 5038.
44 M. s. Dubecký, P. Jurečka, R. Derian, P. Hobza, M. Otyepka and L. Mitas, *J. Chem. Theory Comput.*, 2013, **9**, 4287.
45 M. Dubecký, L. Mitas and P. Jurečka, *Chem. Rev.*, 2016, **116**, 5188.
46 L. K. Wagner, *Int. J. Quantum Chem.*, 2014, **114**, 94.
47 W. Kohn, A. D. Becke and R. G. Parr, *J. Phys. Chem.*, 1996, **100**, 12974.
48 N. Mardirossian and M. Head-Gordon, *Mol. Phys.*, 2017, **115**, 2315.
49 K. Capelle, *Braz. J. Phys.*, 2006, **36**, 1318.
50 S. Kummel and L. Kronik, *Rev. Mod. Phys.*, 2008, **80**, 3.
51 D. Marx and J. Hutter, *Ab initio molecular dynamics: basic theory and advanced methods*, Cambridge University Press, 2009.
52 T. Mueller and G. Ceder, *J. Phys. Chem. B*, 2005, **109**, 17974.
53 P. Srepusharawoot, R. H. Scheicher, C. Moysés Araújo, A. Blomqvist, U. Pinsook and R. Ahuja, *J. Phys. Chem. C*, 2009, **113**, 8498.
54 M. P. Allen and D. J. Tildesley, *Computer simulation of liquids*, Oxford University Press, 2017.
55 D. J. Adams, *Mol. Phys.*, 1975, **29**, 307.
56 S. S. Han, J. L. Mendoza-Cortes and W. A. Goddard III, *Chem. Soc. Rev.*, 2009, **38**, 1460.
57 R. B. Getman, Y.-S. Bae, C. E. Wilmer and R. Q. Snurr, *Chem. Rev.*, 2012, **112**, 703.
58 S. Keskin, J. Liu, R. B. Rankin, J. K. Johnson and D. S. Sholl, *Ind. Eng. Chem. Res.*, 2009, **48**, 2355.
59 E. Tsivion, S. P. Veccham and M. Head-Gordon, *ChemPhysChem*, 2017, **18**, 184.
60 E. Tsivion, J. Long and M. Head-Gordon, *J. Am. Chem. Soc.*, 2014, **136**, 17827.
61 A. Cohen, P. Mori-Sanchez and W. Yang, *Chem. Rev.*, 2012, **112**, 289.
62 M. Bajdich, F. A. Reboredo and P. R. C. Kent, *Phys. Rev. B: Condens. Matter Mater. Phys.*, 2010, **82**, 081405.
63 W. Purwanto, H. Krakauer, Y. Virgus and S. Zhang, *J. Chem. Phys.*, 2011, **135**, 164105.
64 X. Jiang, X. Cheng, G. Chen and H. Zhang, *Int. J. Quantum Chem.*, 2012, **112**, 2627.
65 Y.-H. Kim, Y. Zhao, A. Williamson, M. J. Heben and S. B. Zhang, *Phys. Rev. Lett.*, 2006, **96**, 016102.
66 J. Ma, A. Michaelides and D. Alfè, *J. Chem. Phys.*, 2011, **134**, 134701.
67 B. Vlaisavljevich, J. Huck, Z. Hulvey, K. Lee, J. A. Mason, J. B. Neaton, J. R. Long, C. M. Brown, D. Alfè, A. Michaelides and B. Smit, *J. Phys. Chem. A*, 2017, **121**, 4139.
68 S. Grimme, *J. Comput. Chem.*, 2006, **27**, 1787.
69 J. Chai and M. Head-Gordon, *Phys. Chem. Chem. Phys.*, 2008, **10**, 6615.
70 J. Klimes and A. Michaelides, *J. Chem. Phys.*, 2012, **137**, 120901.
71 S. Dodziuk and G. Dolgonos, *Chem. Phys. Lett.*, 2002, **356**, 79.
72 H. Cheng, A. C. Cooper, G. P. Pez, M. K. Kostov, P. Piotrowski and S. J. Stuart, *J. Phys. Chem. B*, 2005, **109**, 3780.
73 Q. Yang and C. Zhong, *J. Phys. Chem. B*, 2005, **109**, 11862.
74 A. Skoulidas and D. S. Sholl, *J. Phys. Chem. B*, 2005, **109**, 15760.
75 S. Andersson and P. E. Larsson, *Microporous Mesoporous Mater.*, 2016, **224**, 349.
76 D. Durette, P. Benard, R. Zacharia and R. Chahine, *Sci. Bull.*, 2016, **61**, 594.
77 S. Grimme and M. Steinmetz, *Phys. Chem. Chem. Phys.*, 2013, **15**, 16031.
78 S. Grimme, *Wiley Interdiscip. Rev.: Comput. Mol. Sci.*, 2011, **1**, 211.

79 S. Grimme, J. Antony, S. Ehrlich and H. Krieg, *J. Chem. Phys.*, 2010, **132**, 154104.
80 S. Grimme, J. Antony, T. Schwabe and C. Muck-Lichtenfeld, *Org. Biomol. Chem.*, 2007, **5**, 741.
81 J. Antony and S. Grimme, *Phys. Chem. Chem. Phys.*, 2006, **8**, 5287.
82 S. Kristyan and P. Pulay, *Chem. Phys. Lett.*, 1994, **229**, 175.
83 J. Witte, N. Mardirossian, J. B. Neaton and M. Head-Gordon, *J. Chem. Theory Comput.*, 2017, **13**, 2043.
84 E. Caldeweyher, C. Bannwarth and S. Grimme, *J. Chem. Phys.*, 2017, **147**, 034112.
85 J. Wellendorff, K. T. Lundgaard, A. Møgelhøj, V. Petzold, D. D. Landis, J. K. Nørskov, T. Bligaard and K. W. Jacobsen, *Phys. Rev. B: Condens. Matter Mater. Phys.*, 2012, **85**, 235149.
86 Y.-H. Kim, Y. Y. Sun and S. B. Zhang, *Phys. Rev. B: Condens. Matter Mater. Phys.*, 2009, **79**, 115424.
87 H. Lee, J. Ihm, M. L. Cohen and S. G. Louie, *Nano Lett.*, 2010, **10**, 793.
88 M. Dion, H. Rydberg, E. Schröder, D. C. Langreth and B. I. Lundqvist, *Phys. Rev. Lett.*, 2004, **92**, 246401.
89 J. Klimeš, D. R. Bowler and A. Michaelides, *J. Phys.: Condens. Matter*, 2010, **22**, 022201.
90 J. Sun, M. Marsman, G. I. Csonka, A. Ruzsinszky, P. Hao, Y.-S. Kim, G. Kresse and J. P. Perdew, *Phys. Rev. B: Condens. Matter Mater. Phys.*, 2011, **84**, 035117.
91 A. Tkatchenko and M. Scheffler, *Phys. Rev. Lett.*, 2009, **102**, 073005.
92 S. L. Mayo, B. D. Olafson and W. A. Goddard, *J. Phys. Chem.*, 1990, **94**, 8897.
93 W. L. Jorgensen, D. S. Maxwell and J. Tirado-Rives, *J. Am. Chem. Soc.*, 1996, **118**, 11225.
94 T. Pham, K. A. Forrest, J. Eckert and B. Space, *Cryst. Growth Des.*, 2016, **16**, 867.
95 P. R. Horn, Y. Mao and M. Head-Gordon, *Phys. Chem. Chem. Phys.*, 2016, **18**, 23067.
96 Y. Mo, P. Bao and J. Gao, *Phys. Chem. Chem. Phys.*, 2011, **13**, 6760.
97 B. Jeziorski, R. Moszynski and K. Szalewicz, *Chem. Rev.*, 1994, **94**, 1887.
98 H. J. Fang, H. Demir, P. Kamakoti and D. S. Sholl, *J. Mater. Chem. A*, 2014, **2**, 274.
99 J. G. McDaniel and J. R. Schmidt, in *Annual Review of Physical Chemistry*, ed. M. A. Johnson and T. J. Martinez, 2016, vol. 67, pp. 467–488.
100 J. R. Schmidt, K. Yu and J. G. McDaniel, *Acc. Chem. Res.*, 2015, **48**, 548.
101 S. Grimme, *Chem. – Eur. J.*, 2012, **18**, 9955.
102 Y. P. Li, J. Gomes, S. M. Sharada, A. T. Bell and M. Head-Gordon, *J. Phys. Chem. C*, 2015, **119**, 1840.
103 I. Savchenko, B. Gu, T. Heine, J. Jakowski and S. Garashchuk, *Chem. Phys. Lett.*, 2017, **670**, 64.
104 G. Piccini and J. Sauer, *J. Chem. Theory Comput.*, 2014, **10**, 2479.
105 Y. P. Li, A. T. Bell and M. Head-Gordon, *J. Chem. Theory Comput.*, 2016, **12**, 2861.
106 S.-T. Lin, P. K. Maiti and W. A. Goddard III, *J. Phys. Chem. B*, 2010, **114**, 8191.
107 S.-N. Huang, T. A. Pascal, W. A. Goddard III, P. K. Maiti and S.-T. Lin, *J. Chem. Theory Comput.*, 2011, **7**, 1893.
108 B. J. Borah, P. K. Maiti, C. Chakravarty and S. Yashonath, *J. Chem. Phys.*, 2012, **136**, 174510.
109 I. Matanović, J. L. Belof, B. Space, K. Sillar, J. Sauer, J. Eckert and Z. Bacic, *J. Chem. Phys.*, 2012, **137**, 014701.
110 T. Pham, K. A. Forrest, M. Mostrom, J. R. Hunt, H. Furukawa, J. Eckert and B. Space, *Phys. Chem. Chem. Phys.*, 2017, **19**, 13075.
111 L. P. Lindoy, S. J. Kolmann, J. H. D'Arcy, D. L. Crittenden and M. J. T. Jordan, *J. Chem. Phys.*, 2015, **143**, 194302.
112 A. K. Singh, J. Lu, R. S. Aga and B. I. Yakobson, *J. Phys. Chem. C*, 2011, **115**, 2476.
113 R. P. Feynman, A. R. Hibbs and D. F. Styer, *Quantum mechanics and path integrals*, Courier Corporation, 2010.
114 K. Sumida, D. Stück, L. Mino, J. Chai, E. Bloch, O. Zavorotynska, L. Murray, M. Dincă, S. Chavan, S. Bordiga, M. Head-Gordon and J. Long, *J. Am. Chem. Soc.*, 2013, **135**, 1083.
115 P. J. Hasnip, K. Refson, M. I. J. Probert, J. R. Yates, S. J. Clark and C. J. Pickard, *Philos. Trans. R. Soc., A*, 2014, **372**, 20130270.
116 K. Sillar, A. Hofmann and J. Sauer, *J. Am. Chem. Soc.*, 2009, **131**, 4143.
117 A. Kundu, G. Piccini, K. Sillar and J. Sauer, *J. Am. Chem. Soc.*, 2016, **138**, 14047.
118 D. Dutta, B. C. Wood, S. Y. Bhide, K. G. Ayappa and S. Narasimhan, *J. Phys. Chem. C*, 2014, **118**, 7741.
119 D. Henwood and J. D. Carey, *Phys. Rev. B: Condens. Matter Mater. Phys.*, 2007, **75**, 245413.
120 K. Ulman, D. Bhaumik, B. C. Wood and S. Narashimhan, *J. Chem. Phys.*, 2014, **140**, 174708.
121 D. P. Broom and M. Hirscher, *Energy Environ. Sci.*, 2016, **9**, 3368.
122 K. E. Hurst, P. A. Parilla, K. J. O'Neill and T. Gennett, *Appl. Phys. A: Mater. Sci. Process.*, 2016, **122**, 42.
123 J. Park, J. D. Howe and D. S. Sholl, *Chem. Mater.*, 2017, **29**, 10487.
124 S. T. Meek, J. A. Greathouse and M. D. Allendorf, *Adv. Mater.*, 2011, **23**, 249.
125 Y. Sun and H.-C. Zhou, *Sci. Technol. Adv. Mater.*, 2015, **16**, 054202.
126 J. Jiang, Y. Zhao and O. M. Yaghi, *J. Am. Chem. Soc.*, 2016, **138**, 3255.
127 A. J. Howarth, A. W. Peters, N. A. Vermeulen, T. C. Wang, J. T. Hupp and O. K. Farha, *Chem. Mater.*, 2017, **29**, 26.
128 X. Yu, Z. Tang, D. Sun, L. Ouyang and M. Zhu, *Prog. Mater. Sci.*, 2017, **88**, 1.
129 P. A. Julien, C. Mottillo and T. Friščić, *Green Chem.*, 2017, **19**, 2729.
130 J. E. Mondloch, O. Karagiaridi, O. K. Farha and J. T. Hupp, *CrystEngComm*, 2013, **15**, 9258.
131 A. P. Nelson, O. K. Farha, K. L. Mulfort and J. T. Hupp, *J. Am. Chem. Soc.*, 2009, **131**, 458.
132 Y.-P. He, Y.-X. Tan and J. Zhang, *Inorg. Chem.*, 2012, **51**, 11232.
133 B. Liu, A. G. Wong-Foy and A. J. Matzger, *Chem. Commun.*, 2013, **49**, 1419.

134 T. Runčevski, M. T. Kapelewski, R. M. Torres-Gavosto, J. D. Tarver, C. M. Brown and J. R. Long, *Chem. Commun.*, 2016, **52**, 8251.
135 K. J. Gross, K. R. Carrington, S. Barcelo, A. Karkamkar, J. Purewal, S. Ma, H.-C. Zhou, P. Dantzer, K. Ott, T. Burrell, T. Semelsberger, Y. Pivak, B. Dam, D. Chandra and P. Parilla, Recommended Best Practices for the Characterization of Storage Properties of Hydrogen Storage Materials, U.S. Department of Energy, 2012, https://energy.gov/sites/prod/files/2014/03/f12/best_practices_hydrogen_storage.pdf, accessed Mar 2018.
136 D. P. Broom and C. J. Webb, *Int. J. Hydrogen Energy*, 2017, **42**, 29320.
137 H. Oh, T. Gennett, P. Atanassov, M. Kurttepeli, S. Bals, K. E. Hurst and M. Hirscher, *Microporous Mesoporous Mater.*, 2013, **177**, 66.
138 D. DeSantis, J. A. Mason, B. D. James, C. Houchins, J. R. Long and M. Veenstra, *Energy Fuels*, 2017, **31**, 2024.
139 C. O. Areán, S. Chavan, C. P. Cabello, E. Garrone and G. T. Palomino, *ChemPhysChem*, 2010, **11**, 3237.
140 M. Dincă, A. Dailly, Y. Liu, C. M. Brown, D. A. Neumann and J. R. Long, *J. Am. Chem. Soc.*, 2006, **128**, 16876.
141 Y. Liu, C. M. Brown, D. A. Neumann, V. K. Peterson and C. J. Kepert, *J. Alloys Compd.*, 2007, **446-447**, 385.
142 J. Purewal, J. B. Keith, C. C. Ahn, C. M. Brown, M. Tyagi and B. Fultz, *J. Chem. Phys.*, 2012, **137**, 224704.
143 Hydrogen Storage Engineering Center of Excellence Models, http://www.hsecoe.org/models.php, accessed March 2018.
144 A. J. Lachawiec, Jr. and R. T. Yang, *Langmuir*, 2008, **24**, 6159.
145 Y. Li and R. T. Yang, *J. Am. Chem. Soc.*, 2006, **128**, 8136.
146 R. T. Yang and Y. Wang, *J. Am. Chem. Soc.*, 2009, **131**, 4224.
147 M. Suri, M. Dornfeld and E. Ganz, *J. Chem. Phys.*, 2009, **131**, 174703.
148 Y. Zhao and T. Gennett, *Phys. Rev. Lett.*, 2014, **112**, 076101.
149 C. M. Ghimbeau, C. Zlotea, R. Gadiou, F. Cuevas, E. Leroy, M. Latroche and C. Vix-Guterl, *J. Mater. Chem.*, 2011, **21**, 17765.
150 N. P. Stadie, J. J. Purewal, C. C. Ahn and B. Fultz, *Langmuir*, 2010, **26**, 15481.
151 A. Ansón, E. Lafuente, E. Urriolabeitia, R. Navarro, A. M. Benito, W. K. Maser and M. T. Martínez, *J. Phys. Chem. B*, 2006, **110**, 6643.
152 R. Campesi, F. Cuevas, M. Latroche and M. Hirscher, *Phys. Chem. Chem. Phys.*, 2010, **12**, 10457.
153 S. M. Luzan and A. V. Talyzin, *Microporous Mesoporous Mater.*, 2010, **135**, 201.
154 Y. Li, L. Wang and R. T. Yang, *Microporous Mesoporous Mater.*, 2010, **135**, 206.
155 M. Hirscher, *Microporous Mesoporous Mater.*, 2010, **135**, 209.
156 S. M. Luzan and A. V. Talyzin, *Microporous Mesoporous Mater.*, 2011, **139**, 216.
157 M. Dincă and J. R. Long, *Angew. Chem., Int. Ed.*, 2008, **47**, 6766.
158 H. Furukawa, K. E. Cordova, M. O'Keeffe and O. M. Yaghi, *Science*, 2013, **341**, 1230444.
159 B. Chen, M. Eddaoudi, T. M. Reineke, J. W. Kampf, M. O'Keeffe and O. M. Yaghi, *J. Am. Chem. Soc.*, 2000, **122**, 11559.
160 N. L. Rosi, J. Eckert, M. Eddaoudi, D. T. Vodak, J. Kim, M. O'Keeffe and O. M. Yaghi, *Science*, 2003, **300**, 1127.
161 B. Chen, N. W. Ockwig, A. R. Millward, D. S. Contreras and O. M. Yaghi, *Angew. Chem., Int. Ed.*, 2005, **44**, 4745.
162 T. Yildirim and M. R. Hartman, *Phys. Rev. Lett.*, 2005, **95**, 215504.
163 J. G. Vitillo, L. Regli, S. Chavan, G. Ricchiardi, G. Spoto, P. D. C. Dietzel, S. Bordiga and A. Zecchina, *J. Am. Chem. Soc.*, 2008, **130**, 8386.
164 W. Zhou, H. Wu and T. Yildirim, *J. Am. Chem. Soc.*, 2008, **130**, 15268.
165 K. Sumida, C. M. Brown, Z. R. Herm, S. Chavan, S. Bordiga and J. R. Long, *Chem. Commun.*, 2011, **47**, 1157.
166 W. L. Queen, E. D. Bloch, C. M. Brown, M. R. Hudson, J. A. Mason, L. J. Murray, A. J. Ramirez-Cuesta, V. K. Peterson and J. R. Long, *Dalton Trans.*, 2012, **41**, 4180.
167 H. Irving and R. J. P. Williams, *J. Chem. Soc.*, 1953, 3192.
168 A. E. Curzon and A. J. Mascall, *Br. J. Appl. Phys.*, 1965, **16**, 1301.
169 M. T. Kapelewski, T. Runčevski, J. D. Tarver, H. Z. H. Jiang, K. E. Hurst, A. Ayala, T. Gennett, S. A. FitzGerald, C. M. Brown and J. R. Long, submitted.
170 M. Lalonde, W. Bury, O. Karagiaridi, Z. Brown, J. T. Hupp and O. K. Farha, *J. Mater. Chem. A*, 2013, **1**, 5453.
171 S. Das, H. Kim and K. Kim, *J. Am. Chem. Soc.*, 2009, **131**, 3814.
172 X. Song, T. K. Kim, H. Kim, D. Kim, S. Jeong, H. R. Moon and M. S. Lah, *Chem. Mater.*, 2012, **24**, 3065.
173 M. Dincă, W. S. Han, Y. Liu, A. Dailly, C. M. Brown and J. R. Long, *Angew. Chem., Int. Ed.*, 2007, **46**, 1419.
174 X. Solans-Monfort, V. Branchadell, M. Sodupe, C. M. Zicovich-Wilson, E. Gribov, G. Spoto, C. Busco and P. Ugliengo, *J. Phys. Chem. B*, 2004, **108**, 8278.
175 D. Denysenko, M. Grzywa, J. Jelic, K. Reuter and D. Volkmer, *Angew. Chem., Int. Ed.*, 2014, **53**, 5832.
176 M. Witman, S. Ling, A. Gladysiak, K. C. Stylianou, B. Smit, B. Slater and M. Haranczyk, *J. Phys. Chem. C*, 2017, **121**, 1171.
177 T. Arliguie, B. Chaudret, R. H. Morris and A. Sella, *Inorg. Chem.*, 1988, **27**, 598.
178 G. J. Kubas, *Chem. Rev.*, 2007, **107**, 4152.
179 G. J. Kubas, R. R. Ryan, B. I. Swanson, P. J. Vergamini and H. J. Wasserman, *J. Am. Chem. Soc.*, 1984, **106**, 451.
180 G. J. Kubas, *Acc. Chem. Res.*, 1988, **21**, 120.
181 G. J. Kubas, C. J. Burns, G. R. K. Khalsa, L. S. Van Der Sluys, G. Kiss and C. D. Hoff, *Organometallics*, 1992, **11**, 3390.
182 A. F. Borowski, B. Donnadieu, J.-C. Daran, S. Sabo-Etienne and B. Chaudret, *Chem. Commun.*, 2000, 543.
183 M. L. Christ, S. Sabo-Etienne, G. Chung and B. Chaudret, *Inorg. Chem.*, 1994, **33**, 5316.
184 M. Grellier, L. Vendier, B. Chaudret, A. Albinati, S. Rizzato, S. Mason and S. Sabo-Etienne, *J. Am. Chem. Soc.*, 2005, **127**, 17592.
185 M. Grellier, L. Vendier and S. Sabo-Etienne, *Angew. Chem., Int. Ed.*, 2007, **46**, 2613.

186 G. J. Kubas, J. E. Nelson, J. C. Bryan, J. Eckert, L. Wisniewski and K. Zilm, *Inorg. Chem.*, 1994, **33**, 2954.
187 A. Toupadakis, G. J. Kubas, W. A. King, B. L. Scott and J. Huhmann-Vincent, *Organometallics*, 1998, **17**, 5315.
188 M. Dincă and J. R. Long, *J. Am. Chem. Soc.*, 2005, **127**, 9376.
189 L. Sun, T. Miyakai, S. Seki and M. Dincă, *J. Am. Chem. Soc.*, 2013, **135**, 8185.
190 F. Luo, C. Yan, L. Dang, R. Krishna, W. Zhou, H. Wu, X. Dong, Y. Han, T.-L. Hu, M. O'Keeffe, L. Wang, M. Luo, R.-B. Lin and B. Chen, *J. Am. Chem. Soc.*, 2016, **138**, 5678.
191 S. M. Cohen, *Chem. Rev.*, 2012, **112**, 970.
192 D. W. Smithenry, S. R. Wilson and K. S. Suslick, *Inorg. Chem.*, 2003, **42**, 7719.
193 W. Morris, B. Volosskiy, S. Demir, F. Gándara, P. L. McGrier, H. Furukawa, D. Cascio, J. F. Stoddart and O. M. Yaghi, *Inorg. Chem.*, 2012, **51**, 6443.
194 B. Chen, X. Zhao, A. Putkham, K. Hong, E. B. Lobkovsky, E. J. Hurtado, A. J. Fletcher and K. M. Thomas, *J. Am. Chem. Soc.*, 2008, **130**, 6411.
195 C.-D. Wu, A. Hu, L. Zhang and W. Lin, *J. Am. Chem. Soc.*, 2005, **127**, 8940.
196 E. D. Bloch, D. Britt, C. Lee, C. J. Doonan, F. J. Uribe-Romo, H. Furukawa, J. R. Long and O. M. Yaghi, *J. Am. Chem. Soc.*, 2010, **132**, 14382.
197 C. J. Doonan, W. Morris, H. Furukawa and O. M. Yaghi, *J. Am. Chem. Soc.*, 2009, **131**, 9492.
198 K. K. Tanabe, C. A. Allen and S. M. Cohen, *Angew. Chem., Int. Ed.*, 2010, **49**, 9730.
199 K. Koh, A. G. Wong-Foy and A. J. Matzger, *Angew. Chem., Int. Ed.*, 2008, **47**, 677.
200 H. Fei, J.-W. Shin, Y. S. Meng, M. Adelhardt, J. Sutter, K. Meyer and S. M. Cohen, *J. Am. Chem. Soc.*, 2014, **136**, 4965.
201 H. G. T. Nguyen, M. H. Weston, A. A. Sarjeant, D. M. Gardner, Z. An, R. Carmieli, M. R. Wasielewski, O. K. Farha, J. T. Hupp and S.-B. T. Nguyen, *Cryst. Growth Des.*, 2013, **13**, 3528.
202 U. H. F. Bunz, K. Seehafer, F. L. Geyer, M. Bender, I. Braun, E. Smarsly and J. Freudenberg, *Macromol. Rapid Commun.*, 2014, **35**, 1466.
203 S. Das, P. Heasman, T. Ben and S. Qiu, *Chem. Rev.*, 2017, **117**, 1515.
204 T. Ben, H. Ren, S. Ma, D. Cao, J. Lan, X. Jing, W. Wang, J. Xu, F. Deng, J. M. Simmons, S. Qiu and G. Zhu, *Angew. Chem., Int. Ed.*, 2009, **48**, 9457.
205 W. Lu, D. Yuan, D. Zhao, C. I. Schilling, O. Plietzsch, T. Muller, S. Bräse, J. Guenther, J. Blümel, R. Krishna, Z. Li and H.-C. Zhou, *Chem. Mater.*, 2010, **22**, 5964.
206 D. Yuan, W. Lu, D. Zhao and H.-C. Zhou, *Adv. Mater.*, 2011, **23**, 3723.
207 C. Pei, T. Ben, Y. Li and S. Qiu, *Chem. Commun.*, 2014, **50**, 6134.
208 H. M. El-Kaderi, J. R. Hunt, J. L. Mendoza-Cortés, A. P. Côté, R. E. Taylor, M. O'Keeffe and O. M. Yaghi, *Science*, 2007, **316**, 268.
209 J. M. H. Thomas and A. Trewin, *J. Phys. Chem. C*, 2014, **118**, 19712.
210 P. Fayon and A. Trewin, *Phys. Chem. Chem. Phys.*, 2016, **18**, 16840.
211 A. Tarzia, A. W. Thornton, C. J. Doonan and D. M. Huang, *J. Phys. Chem. C*, 2017, **121**, 16381.
212 J.-X. Jiang, C. Wang, A. Laybourn, T. Hasell, R. Clowes, Y. Z. Khimyak, J. Xiao, S. J. Higgins, D. J. Adams and A. I. Cooper, *Angew. Chem., Int. Ed.*, 2011, **50**, 1072.
213 Y. Xie, T.-T. Wang, X.-H. Liu, K. Zou and W.-Q. Deng, *Nat. Commun.*, 2013, **4**, 1960.
214 N. B. McKeown, S. Hanif, K. Msayib, C. E. Tattershall and P. M. Budd, *Chem. Commun.*, 2002, 2782.
215 M. H. Weston, O. K. Farha, B. G. Hauser, J. T. Hupp and S.-B. T. Nguyen, *Chem. Mater.*, 2012, **24**, 1292.
216 S. Fischer, J. Schmidt, P. Strauch and A. Thomas, *Angew. Chem., Int. Ed.*, 2013, **52**, 12174.
217 A. P. Côté, A. I. Benin, N. W. Ockwig, M. O'Keeffe, A. J. Matzger and O. M. Yaghi, *Science*, 2005, **310**, 1166.
218 J. R. Hunt, C. J. Doonan, J. D. LeVangie, A. P. Côté and O. M. Yaghi, *J. Am. Chem. Soc.*, 2008, **130**, 11872.
219 F. J. Uribe-Romo, J. R. Hunt, H. Furukawa, C. Klöck, M. O'Keeffe and O. M. Yaghi, *J. Am. Chem. Soc.*, 2009, **131**, 4570.
220 P. Kuhn, M. Antonietti and A. Thomas, *Angew. Chem., Int. Ed.*, 2008, **47**, 3450.
221 K. T. Jackson, T. E. Reich and H. M. El-Kaderi, *Chem. Commun.*, 2012, **48**, 8823.
222 J. W. Colson and W. R. Dichtel, *Nat. Chem.*, 2013, **5**, 453.
223 G. Lin, H. Ding, D. Yuan, B. Wang and C. Wang, *J. Am. Chem. Soc.*, 2016, **138**, 3302.
224 A. P. Côté, H. M. El-Kaderi, H. Furukawa, J. R. Hunt and O. M. Yaghi, *J. Am. Chem. Soc.*, 2007, **129**, 12914.
225 H. Furukawa and O. M. Yaghi, *J. Am. Chem. Soc.*, 2009, **131**, 8875.
226 Z. Li, X. Feng, Y. Zou, Y. Zhang, H. Xi, X. Liu and Y. Mu, *Chem. Commun.*, 2014, **50**, 13825.
227 X. Feng, L. Liu, Y. Honsho, A. Saeki, S. Seki, S. Irle, Y. Dong, A. Nagai and D. Jiang, *Angew. Chem., Int. Ed.*, 2012, **51**, 2618.
228 S.-Y. Ding, J. Gao, Q. Wang, Y. Zhang, W.-G. Song, C.-Y. Su and W. Wang, *J. Am. Chem. Soc.*, 2011, **133**, 19816.
229 W. Zhang, P. Jiang, Y. Wang, J. Zhang, Y. Gao and P. Zhang, *RSC Adv.*, 2014, **4**, 51544.
230 S. B. Kalidindi, K. Yusenko and R. A. Fischer, *Chem. Commun.*, 2011, **47**, 8506.
231 S. B. Kalidindi, H. Oh, M. Hirscher, D. Esken, C. Wiktor, S. Turner, G. Van Tendeloo and R. A. Fischer, *Chem. – Eur. J.*, 2012, **18**, 10848.
232 B. Szczęśniak, J. Choma and M. Jaroniec, *Adv. Colloid Interface Sci.*, 2017, **243**, 46.
233 S. Zhu and T. Li, *ACS Nano*, 2014, **8**, 2864.
234 T. H. Kim, J. Bae, T. H. Lee, J. Hwang, J. H. Jung, D. K. Kim, J. S. Lee, D. O. Kim, Y. H. Lee and J. Ihm, *Nano Energy*, 2016, **27**, 402.
235 J. W. Burress, S. Gadipelli, J. Ford, J. M. Simmons, W. Zhou and T. Yildirim, *Angew. Chem., Int. Ed.*, 2010, **49**, 8902.
236 A. G. Klechikov, G. Mercier, P. Merino, S. Blanco, C. Merino and A. V. Talyzin, *Microporous Mesoporous Mater.*, 2015, **210**, 46.

237 E. Beheshti, A. Nojeh and P. Servati, *Carbon*, 2011, **49**, 1561.
238 C.-H. Chen, T.-Y. Chung, C.-C. Shen, M.-S. Yu, C.-S. Tsao, G.-N. Shi, C.-C. Huang, M.-D. Ger and W.-L. Lee, *Int. J. Hydrogen Energy*, 2013, **38**, 3681.
239 C. Zhou, J. A. Szpunar and X. Cui, *ACS Appl. Mater. Interfaces*, 2016, **8**, 15232.
240 A. C. Dillon, K. M. Jones, T. A. Bekkedahl, C. H. Kiang, D. S. Bethune and M. J. Heben, *Nature*, 1997, **386**, 377.
241 C. Liu, Y. Chen, C.-Z. Wu, S.-T. Xu and H.-M. Cheng, *Carbon*, 2010, **48**, 452.
242 H. J. Wasserman, G. J. Kubas and R. R. Ryan, *J. Am. Chem. Soc.*, 1986, **108**, 2294.
243 L. F. Wang, F. H. Yang and R. T. Yang, *AIChE J.*, 2009, **55**, 1823.
244 Y. Jeong and T. C. M. Chung, *Carbon*, 2010, **48**, 2526.
245 Z. Jin, Z. Z. Sun, L. J. Simpson, K. J. O'Neill, P. A. Parilla, Y. Li, N. P. Stadie, C. C. Ahn, C. Kittrell and J. M. Tour, *J. Am. Chem. Soc.*, 2010, **132**, 15246.

